UNIVERSITY OF SOUTHERN CALIFORNIA

SCHOOL OF ENGINEERING

UNIVERSITY RESEARCH INITIATIVE

CENTER FOR THE INTEGRATION OF OPTICAL COMPUTING

AFOSR-90-0133

FINAL TECHNICAL REPORT

FOR THE PERIOD

February 15, 1992 through August 14, 1993

Presented To:

Air Force Office of Scientific Research
Building 410
Attn:. XOT (Room A115)
Bolling AFB, DC 20332-6448

Presented By:

University of Southern California
School of Engineering
Los Angeles, California 90089-0483

Principal Investigators

A. A. Sawchuk and W. H. Steier

1. AGENCY USE ONLY (Leave blank)	2. REPORT DATE	3. REPORT TYPE AND DATES COVERED
	10/15/93	FINAL TECHNICAL REPORT 2/15/90-8/14/93

4. TITLE AND SUBTITLE
CENTER FOR THE INTEGRATION OF OPTICAL COMPUTING

5. FUNDING NUMBERS
AFOSR 90-0133

6. AUTHOR(S)
PRINCIPAL INVESTIGATORS:
A. A. SAWCHUK - W. H. STEIER

7. PERFORMING ORGANIZATION NAME(S) AND ADDRESS(ES)
UNIVERSITY OF SOUTHERN CALIFORNIA
DEPT. OF ELECTRICAL/ ELECTROPHYSICS ENGINEERING
SEAVER SCIENCE CENTER 502
LOS ANGELES, CA 90089/0483

8. PERFORMING ORGANIZATION REPORT NUMBER

9. SPONSORING/MONITORING AGENCY NAME(S) AND ADDRESS(ES)
AIR FORCE OFFICE OF SCIENTIFIC RESEARCH
BUILDING 410
BOLLING AIR FORCE BASE
DC 20332-6448

10. SPONSORING/MONITORING AGENCY REPORT NUMBER
3480A3

11. SUPPLEMENTARY NOTES

12a. DISTRIBUTION/AVAILABILITY STATEMENT
unlimited

12b. DISTRIBUTION CODE

13. ABSTRACT (Maximum 200 words)

Topics reviewed include: Optical interconnections, lenslet array processors, generalizable neural networks, spatial light modulators. MBE growth of quantum well structures, ultralow threshold arrays, charge transport optical nonlinearities, Ebium-doped amplifiers in optical switching systems.

14. SUBJECT TERMS	15. NUMBER OF PAGES
OPTICAL COMPUTING, LASER ARRAYS, SPATIAL MODULATORS, OPTICAL INTERCONNECTIONS, OPTICAL NEURAL INTERCONNECTIONS	70
	16. PRICE CODE

17. SECURITY CLASSIFICATION OF REPORT	18. SECURITY CLASSIFICATION OF THIS PAGE	19. SECURITY CLASSIFICATION OF ABSTRACT	20. LIMITATION OF ABSTRACT
unclass	unclass	unclass	UL

UNIVERSITY RESEARCH INITIATIVE

CENTER FOR THE INTEGRATION OF OPTICAL COMPUTING

AFOSR-90-0133

FINAL TECHNICAL REPORT

FOR THE PERIOD

February 15, 1992 through August 14, 1993

Presented To:

Air Force Office of Scientific Research
Building 410
Attn:. XOT (Room A115)
Bolling AFB, DC 20332-6448

Presented By:

University of Southern California
School of Engineering
Los Angeles, California 90089-0483

Principal Investigators

A. A. Sawchuk and W. H. Steier

TABLE OF CONTENTS

DIRECTOR'S OVERVIEW

This report summarizes the progress made under the University Research Initiative Center for the Integration of Optical Computing. Contract AFOSR 990-0133 for the period 2/15/90 through 8/14/93. This is the final report which summarizes the progress made over the entire contract period. It includes the work of ten faculty from the Departments of Electrical Engineering-Systems, Electrical Engineering - Electrophysics, Materials Science, and Physics.

This report closes with a listing of the publication and presentations of the faculty during the contract period concerning the research on optical computing. As shown by the very large number of publications and presentations listed, this has been a very productive program.

Dynamic Optical Interconnection Networks with Integrated Optoelectronic Transceivers

A. A. Sawchuk and S. R. Forrest

In this program we have developed several new architectures for implementing dynamic optical multistage networks. These architectures take advantage of the volume (3-D) physical nature of optics and implement the network by cascaded stages of 2-D planes [1]- [3]. Figure 1 shows an example called a 3-D folded shuffle network. A 2-D array of input signals enters from the left and is permuted in a fixed pattern by free-space interconnection optics. The signal array then impinges on an array of dynamically reconfigurable optoelectronic bypass/exchange switches, one of which is shown schematically in Fig. 2. In Fig. 1, the detector and source planes of the switches are shown separated for clarity. In the least complex version of these switches, the detectors on one side of the optoelectronic chip detect the signal, where they are either passed straight through (a bypass interconnection), or reversed (exchange interconnection) under external optical or electrical control. The signals are then regenerated and drive a diode laser or optoelectronic modulator for input to the next stage. The optoelectronic switches can also be powered optically, giving many advantages in noise and crosstalk reduction. This cascade of fixed optical permutations and dynamic optoelectronic switches is repeated to make the multiple stages of the network. We have defined new architectures that are well matched to the physical capabilities of optics and optoelectronics to combine these technologies for mutual benefit. We have completed several studies on the mathematical transformation between 2-D (planar) and 3-D (volume) physical networks and their permutation capabilities, and derived mathematical transformations which translate into light-efficient shuffle optics implemented with refractive and diffractive components [1]-[6].

Refractive optics arranged as lenslet arrays can implement the fixed shuffles [6]. This approach works well at near-infrared wavelengths where semiconductor lasers commonly operate. We have evaluated optical limits on the packing density of data lines in a perfect shuffle interconnection network that uses simple spherical lens arrays. We have developed optical design techniques to maximize packing density. Diffraction and geometrical aberrations make opposing demands on the system when trying to achieve smaller spot sizes, and we have used an iterative design procedure to choose the best aperture size and the best physical size for the source (and detector) array. We derived a relationship between the focal length of the lens used and the resolution limit (i.e. the smallest image spots attainable) for our optical perfect shuffle. We have developed a simple model for optical crosstalk in the array, and can predict crosstalk versus inter-detector spacing. Given an acceptable level of crosstalk, we can predict the minimum detector spacing. The optical limits permit several tens of thousands of data channels per square centimeter of the 2-D input and output arrays assuming typical optical components [6]. On the other hand, a much more stringent practical limit results from the power dissipation of the optoelectronic integrated circuitry.

Another method of implementing fixed shuffles uses partially shift-variant holographic optics, and is 100% optically efficient in theory. We have demonstrated

the principle using silver halide holograms and using DuPont holographic transmission photopolymer material. We have achieved more than 60% effective light efficiency after considering the absorption and the reflection of the material. In this experiment, the light efficient algorithm illustrated in Fig. 3 is used. The input plane is first magnified twice. A four facet hologram is used as a holographic prism array to perform different deflection operations on the four quadrants of the magnified input. The four quadrants are deflected and superimposed on the output plane as a 2-D perfect shuffled result.

Figure 4 shows the experimental setup. The two beams shown shaded are used to make the facet hologram on the hologram plane. A specially designed mask at the hologram plane allows only one quadrant to be exposed at a time. We adjust lens L_4 in both horizontal and vertical directions for each exposure to get different deflection angles for each facet. In reconstruction, the reference beam is blocked, and the pre-magnified input plane is inserted. The 4-f optical system projects the four quadrants on the corresponding facets of the hologram. The superposition of these four deflected quadrants appears at the observation plane and shows the shuffled result. The pre-magnified input plane is an 8x8 binary inverse perfect shuffled letter *H*. It is generated by computer and photoreduced to get a 10 mm x 10 mm pattern. Thus, each pixel has diameter 0.31 mm and the center-to-center distance between two neighboring pixels is 1.25 mm.

From our measurements, we found the optimum exposure energy for DuPont photopolymer is approximately 100 mJ/cm^2. The photopolymer hologram needs a UV curing process, which polymerizes the monomers not exposed to light. The fixing energy is around 577 mJ/cm^2. The changes in the exposure energy and the fixing energy influence the final diffraction efficiency of a hologram. In our experiment, the optimum exposure energy for each facet is applied. After the recording, the photopolymer hologram is cured by a UV light source but the fixing energy is not optimized. The real diffraction efficiency, which is defined as the ratio of the intensity of the diffracted light to the incident light, is found to be 60% averaged over the four facets. The scattering of the photopolymer is around 21% and the reflection loss is about 9.2%. However, the effective diffraction efficiency, which is defined to be the ratio of the diffracted light to the sum of the diffracted and the zeroth order light, is measured to be 93.8% on average.

This result demonstrated that high light efficiency optical 2-D perfect shuffles can be achieved when a high optical efficiency algorithm is used in combination with proper optical components. Parameters such as the exposure and fixing energies for hologram preparation must be optimized to get high efficiency.

The work on interconnection architectures has been accompanied by significant progress in the area of optoelectronic optical logic circuits using optical powering [3], [7]-[9]. We found that the performance of high density, high bandwidth 2D and 3D optoelectronic interconnections used in optical processing, computing and communications systems is ultimately limited by crosstalk between neighboring functional elements (or pixels) on the arrays which commonly comprise such interconnection architectures. Crosstalk can have numerous sources, including thermal, optical and electrical. In general, the high frequency performance limit of

many optoelectronic 2D pixel arrays is set by electrical crosstalk to lie in the 200 MHz–500 MHz range. We have concentrated on investigating architectures which are *not* intrinsically limited by crosstalk induced by capacitive and inductive coupling between neighboring pixels. Our approach has been to consider the use of optical sources as a means to apply power independently to each pixel in a large-scale, 2D array. In practice, this is accomplished by integrating a photovoltaic cell array along with each optoelectronic pixel, and then illuminating the cell with a high power GaAs laser diode. Supplying local power in this manner has the advantage of providing an inductance and capacitance-free power source.(i.e., photons), and it eliminates space-consuming power supply lines and capacitive decoupling circuitry at each pixel. In a recent analysis of such a system [9], it was found that optically powered 2D optoelectronic switching arrays can be operated at frequencies at least one order of magnitude higher than similar arrays which are electrically powered.

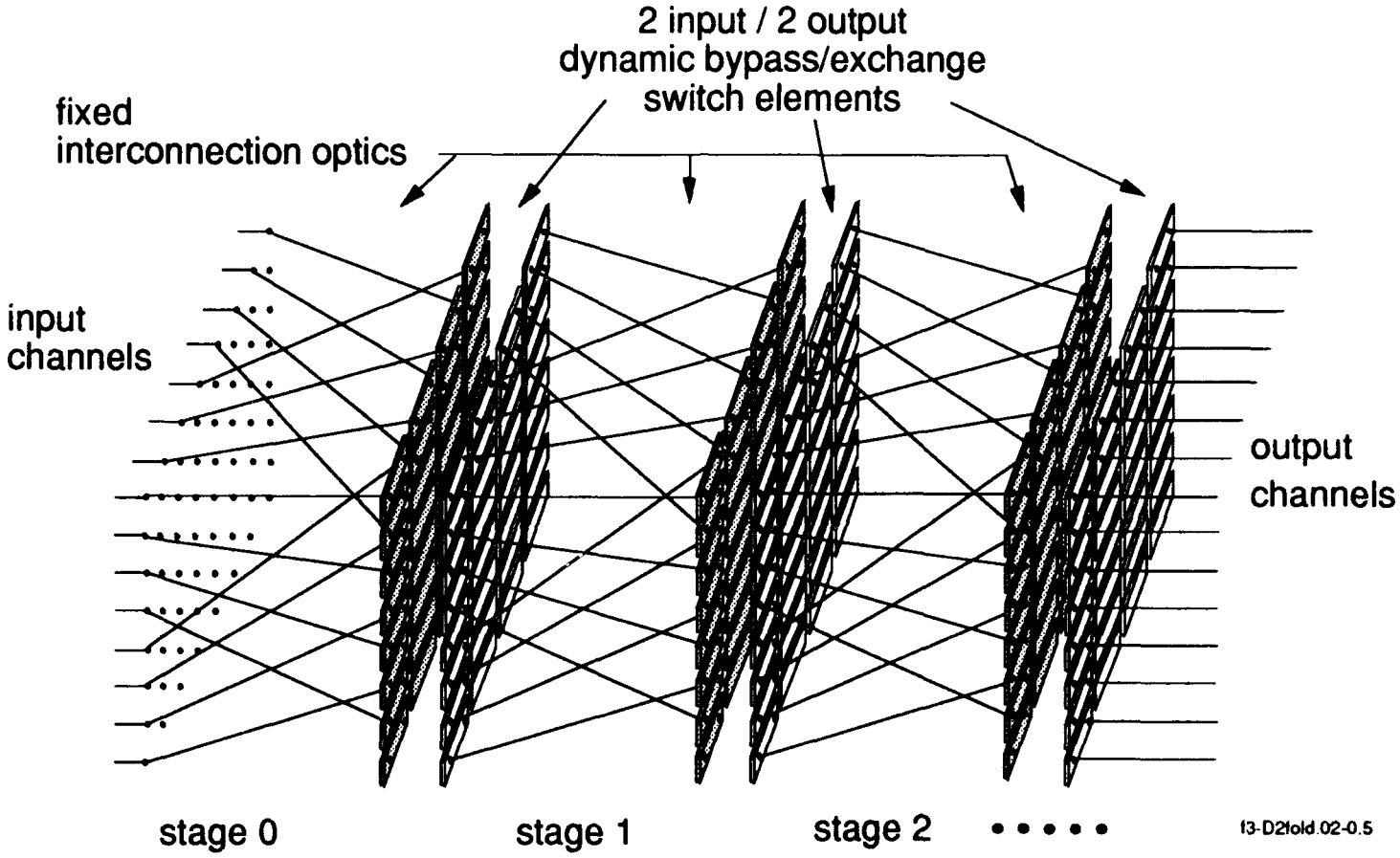

Figure 1. 3-D folded shuffle interconnection network.

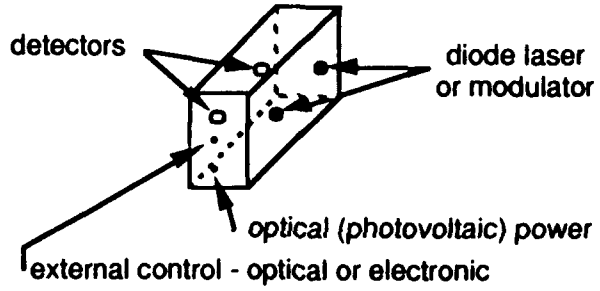

Figure 2. 2-input 2-output optoelectronic switch modules for a folded perfect shuffle network.

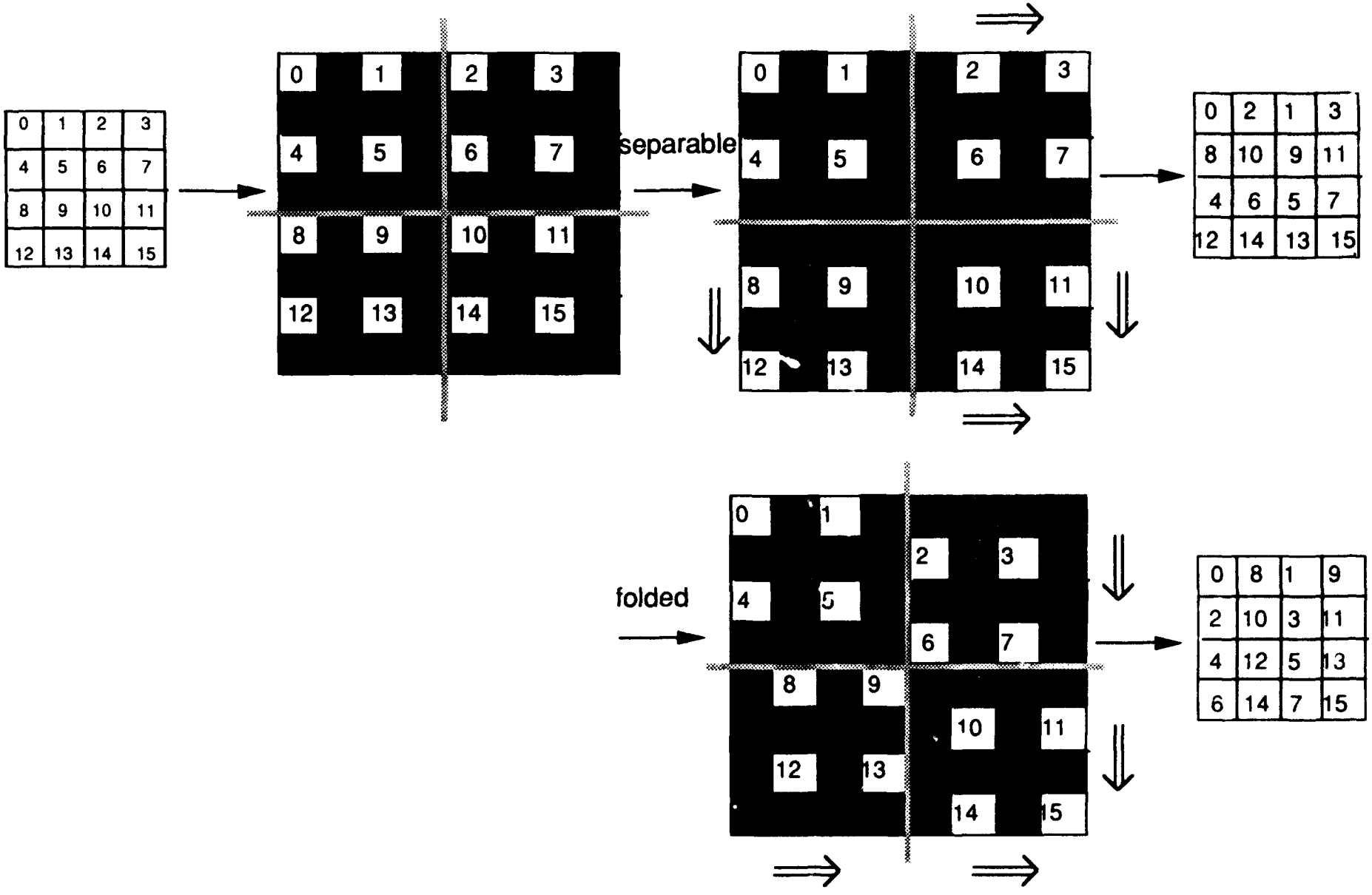

Fig. 3. Schematic representation of the light efficient one-copy shuffle algorithm.

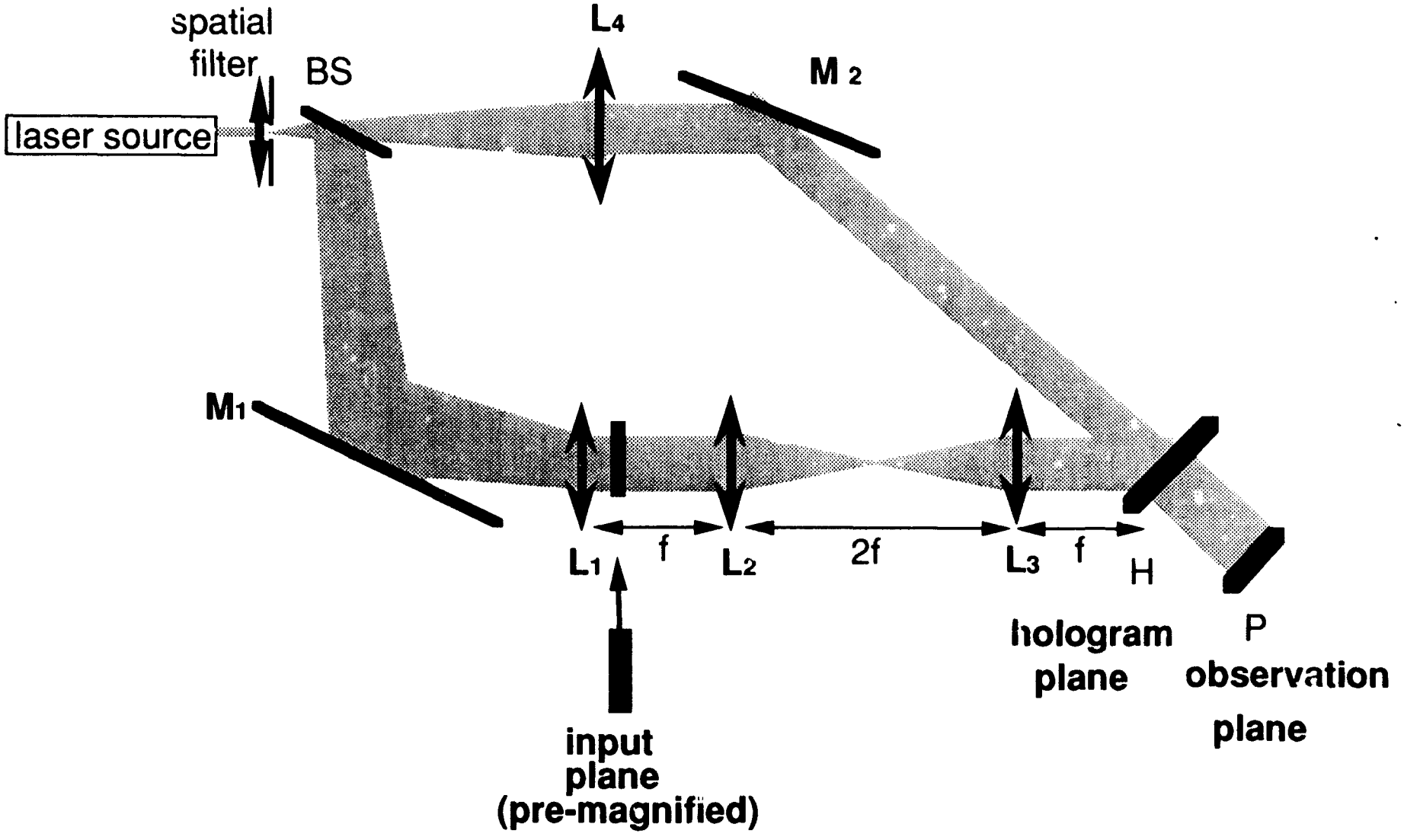

Fig. 4. Experimental setup for making a facet hologram used in the one-copy shuffle algorithm.

Interconnections and Spatial Light Modulators for Generalizable Photonic Neural Networks

Armand R. Tanguay, Jr.

The research project described in this report is one of three collaborative efforts incorporated under the task "Generalizable Photonic Neural Networks" within the University Research Initiative "Center for the Integration of Optical Computing". The other two related and complementary research projects are "Architectures for Generalizable Photonic Neural Networks" (Prof. B. Keith Jenkins), and "MBE Growth of Quantum Well Structures for Generalizable Photonic Neural Networks" (Prof. Anupam Madhukar).

The overall goal of these three highly integrated research efforts was the development of a viable, synthetic, and integrated photonic technology for the implementation of low power, compact, massively parallel, generalizable neural network architectures. Such a technology must be manufacturable, flexible in design, and heavily leveraged by related research and development thrusts. Further, the array of chosen components must be inherently compatible and complementary in form and function. To this end, we have addressed during the contract period a number of key research and development issues that will delineate the future impact of photonic neural networks, as outlined below.

The architecture that we investigated for photonic neural network implementations is shown schematically in Fig. 1. A volume holographic medium is utilized to allow for the required high density of interconnections among the neuron units; this medium may be fixed in the case of a trained network suitable for performing certain tasks based on *a priori* knowledge, or dynamic in the case of a neural network that incorporates a learning algorithm. In order to alleviate several problematic sources of crosstalk and throughput loss that have been characteristic of previously proposed holographic interconnection schemes, a two-dimensional source array of individually coherent but mutually incoherent sources is incorporated to provide for parallel recording of the desired interconnection patterns and weight updates. The corresponding optical system is arranged to transform the spatially distributed source array into sets of angularly multiplexed signal and reference beams that are pairwise coherent, but mutually incoherent to eliminate the potential for coherent recording crosstalk. This double angular multiplexing scheme also eliminates a major source of throughput loss that results from beam degeneracy crosstalk. Two spatial light modulators complete the architecture, representing the neuron unit outputs (SLM_1) and the neuron unit inputs (SLM_2).

In the recording mode of operation, characteristic for example of a learning or training cycle, the shutter in the upper arm of the architecture is open, and both signal ($\{y_i\}$) and reference (x_j) beams generated by a given source within the source array are incident on the volume holographic recording medium. The simultaneous availability of a coherent source beam from each source provides for a full set of weight updates over all of the input values x_j. In the readout or computational mode of operation, the shutter in the upper arm is closed, and reconstruction of the full set of weighted interconnections is provided by means of the source array in conjunction

with SLM_2. Feedback of the reconstructed interconnection matrix to SLM_1 is provided by a combination of mirrors, lenses, and inverting prisms, as shown in Fig. 1. Such feedback can be provided to either the upper arm, the lower arm, or both as demanded by the particular neural network architecture implemented.

During the research program, significant progress has been made in the analysis and quantization of crosstalk and throughput performance achievable in the conventional and incoherent/coherent double angularly multiplexed holographic recording and reconstruction schemes, in the analysis and experimental demonstration of the temporal correlation behavior of dynamic (photorefractive crystal) holographic recording media for implementation of dynamic link neural network concepts, in the demonstration of a novel single step copying technique for multiplexed volume holograms that allows for efficient copying of a fully trained set of interconnection holograms, in the implementation and characterization of neuron unit circuitry capable of providing the appropriate optical detection and functional transformation required in each SLM neuron unit, in the analysis of the technological limitations and design considerations that apply to multiple quantum well (MQW) SLM modulator elements, and in the fabrication and characterization of large area hybridization-compatible SLM modulator element arrays that exhibit a relatively high contrast ratio and dynamic range. In addition, we have further developed the high contrast ratio parallel readout capability of optical disc based spatial light modulators for possible incorporation as training pattern generators in such generalizable photonic neural networks. Each of these advances is described in more detail below.

During the contract period, we have extended our preliminary analyses of reconstruction fidelity and optical throughput for the volume holographic interconnection techniques utilized in the double angularly multiplexed and conventional photonic neural network architectures. This has included the use of the optical beam propagation method to numerically model independent interconnection weights and increased numbers of interconnections (compared to our initial modeling studies), as well as the simulation of the subhologram version of the double angularly multiplexed architecture. In addition, we have considered a comprehensive set of recording methods for the conventional interconnection architecture, which has revealed a potentially serious difficulty in the oft-proposed method of using a page-wise sequential recording technique to reduce the influence of cross gratings on the recorded interconnection pattern. This method (in a conventional architecture) requires very large beam ratios between the reference and image beams in order to avoid inadvertent strengthening of the cross gratings. The required beam ratio scales as N^2 for an N-to-N interconnection system, which is impractical for large N.

Sample simulation results based on the optical beam propagation method are shown in Fig. 2 for both the conventional architecture (for several possible recording methods and readout with mutually coherent beams) and the subhologram version of the double angularly multiplexed architecture. In this figure, the RMS error of the diffracted outputs of a ten-to-ten interconnection is shown as a function of the optical throughput, which is defined as the fraction of incident readout light that is diffracted into the desired outputs. The peak throughput achieved for each case occurs at the right-hand end of each curve. As illustrated in the figure, simultaneous recording of each training pair in a conventional architecture results in large fidelity errors in the

diffracted outputs due to the occurrence of extraneous cross gratings. Reduction or elimination of these cross gratings using page-wise sequential or fully sequential recording techniques can improve reconstruction fidelity (and peak throughput), but at the cost of a significantly larger number of exposures to achieve the desired interconnections. For example, fully sequential recording results in good reconstruction fidelity (as shown in Fig. 2), but requires N^2 more exposures than simultaneous recording. The double angularly multiplexed architecture, however, achieves comparable reconstruction fidelity to sequential recording in a conventional architecture while requiring only one exposure for each training pair. Low interchannel crosstalk is therefore achievable while taking full advantage of the parallelism inherent in optical interconnections to perform the requisite weight updates in adaptive neural networks.

One of the advanced neural network algorithms that we are investigating for implementation in a modified version of the double angularly multiplexed architecture is based on the dynamic link concepts proposed by Prof. Christoph von der Malsburg (Depts. of Computer Science and Electrical Engineering-Systems at USC). A key feature of the dynamic link architecture is the formation of interconnection weights based on the temporal correlation between time varying neuron unit outputs. We have investigated the use of photorefractive media as interconnection elements in which the interconnection weights are related to the *correlations* among pairs of time-varying grating writing beams. Using a charge transport model of photorefractive grating formation, we have obtained analytic solutions for the effective modulation depth of gratings written in the low modulation depth regime, and numerical solutions when the modulation depth is large. Excellent agreement between these solutions and experiments using single crystal bismuth silicon oxide ($Bi_{12}SiO_{20}$) have been obtained. By utilizing the large temporal bandwidths available in our hybrid-integrated SLM arrays and incorporating photorefractive correlating interconnection elements, very high processing throughput for photonic implementations of the dynamic link architecture may be achievable.

One of the most significant problems inherent in neural network implementations has been the difficulty involved in copying a learned interconnection pattern from a master interconnection to one or more identical copies. This capability is essential for both military and commercial viability of any but the simplest neural network implementations, as the training sequence can in many cases prove to be the rate limiting step. In addition, the weights that result from a particular learning sequence may not be known, and in the case of large scale networks, may not prove measurable in finite time if at all. We have shown that the double angularly multiplexed, incoherent/coherent recording and reconstruction geometry for incorporation of holographic interconnection weights is uniquely suited to a single step copying process that allows for reproduction of a fully multiplexed master hologram. Single step copying of multiplexed volume holograms has been demonstrated experimentally in collaboration with Prof. Jenkins' research group. In these experiments, three superposed holograms (each of a single letter) were successfully copied from a master hologram implemented in DuPont's Omnidex photopolymer material to a second photopolymer copy hologram in a single recording step.

During the contract period, we have invented a novel hybrid spatial light modulator configuration that allows for *face-to-face* contact by flip-chip bonding techniques between a silicon chip that incorporates dual channel detectors and control electronics that implement a dual channel sigmoidal transfer function, and a compound semiconductor chip that incorporates an array of multiple quantum well spatial light modulation elements. By utilizing standard CAD design tools and SPICE circuit simulations, we have designed and evaluated appropriate silicon CMOS circuitry using the 2 μm design rules allowed within the MOSIS CMOS design repertoire. To date, functional 6 x 6 arrays of 100 μm square pixels have been successfully fabricated and evaluated that exhibit a high degree of transfer function uniformity across the array. Operational bandwidths in excess of 4 MHz (large signal) and 14 MHz (small signal) have been successfully demonstrated. A new circuit is currently being designed with projected 20 nsec rise and fall times. It will accommodate the 0.5 volt input signal generated by the integrated optical detectors and is designed to operate with an increased output voltage swing of 10 volts, which is compatible with the drive requirements of the multiple quantum well compound semiconductor spatial light modulators discussed below.

Extensive analyses of multiple quantum well based spatial light modulation elements have been undertaken to establish the technological limitations and design constraints characteristic of the asymmetric Fabry-Perot optical cavity geometry, which is often employed to enhance both the contrast ratio and dynamic range of thin MQW modulator structures. These analyses have pointed out the exceptionally high degree of growth thickness uniformity required both within the multiple quantum well region itself, as well as in the incorporated Bragg mirrors that comprise the Fabry-Perot cavity. In these studies, the material systems investigated have included both AlGaAs/GaAs and strained layer InGaAs/GaAs, with the latter system of particular interest due to its capability for growth on a *transparent* GaAs substrate. Such a structure is highly desirable for incorporation in a flip-chip bonded hybrid Si/GaAs spatial light modulator structure, as described above. In collaboration with Prof. Madhukar's research group, large area arrays of InGaAs/GaAs multiple quantum well structures have been fabricated in asymmetric Fabry-Perot cavities by molecular beam epitaxial (MBE) growth techniques, resulting in contrast ratios as high as 66:1 with a dynamic range of 30%. In addition, an *inverted* asymmetric Fabry-Perot cavity multiple quantum well modulator has been fabricated and evaluated that exhibits a contrast ratio of 12:1 and a dynamic range of 20% at 9565 Å. In this novel structure, the *low* reflectivity Bragg mirror is grown first, followed by the multiple quantum well region. An externally-deposited high reflectivity dielectric mirror completes the cavity, reducing the total MBE growth time significantly while allowing for *ex situ* post-growth tuning of the cavity resonance. Such externally-deposited high reflectivity dielectric mirrors have been incorporated both in test Fabry-Perot cavities without active multiple quantum well structures, and in Fabry-Perot cavities with multiple quantum well structures that are maximally detuned from the optimal cavity thickness by growth thickness variations. Retuning of all of the cavities to the desired optimal cavity phasing conditions has been successfully demonstrated, and repeatability and sensitivity measurements have demonstrated an overall *ex situ* cavity tuning accuracy of 20 Å in thickness.

Finally, we have utilized a novel differential interferometric readout technique to allow parallel access to 1 cm^2 images written directly onto optical disc media by area

encoding techniques, with image sizes of 512 x 512 superpixels and an enhanced output contrast ratio of up to 100:1. This achievement has been made possible by the use of glass (as opposed to acrylic) optical disc substrates, as well as by the development (in conjunction with Apex Systems, Inc. in Boulder, Colorado) of a novel optical disc media tester that allows for submicron positioning accuracy of each subpixel bit over very large areas on the optical disc. Using this optical media tester, we have successfully recorded and read out complex pictorial gray scale images with excellent image fidelity and throughput linearity. Throughput linearity has been examined both experimentally by recording patterns with different duty cycles within each superpixel, and theoretically by utilization of the optical beam propagation method. Incorporation of the rotational motion characteristic of optical disc drives allows for the high speed presentation of very large numbers of training images to a neural network. Further applications of this emerging technology to neural network systems are under continuing investigation.

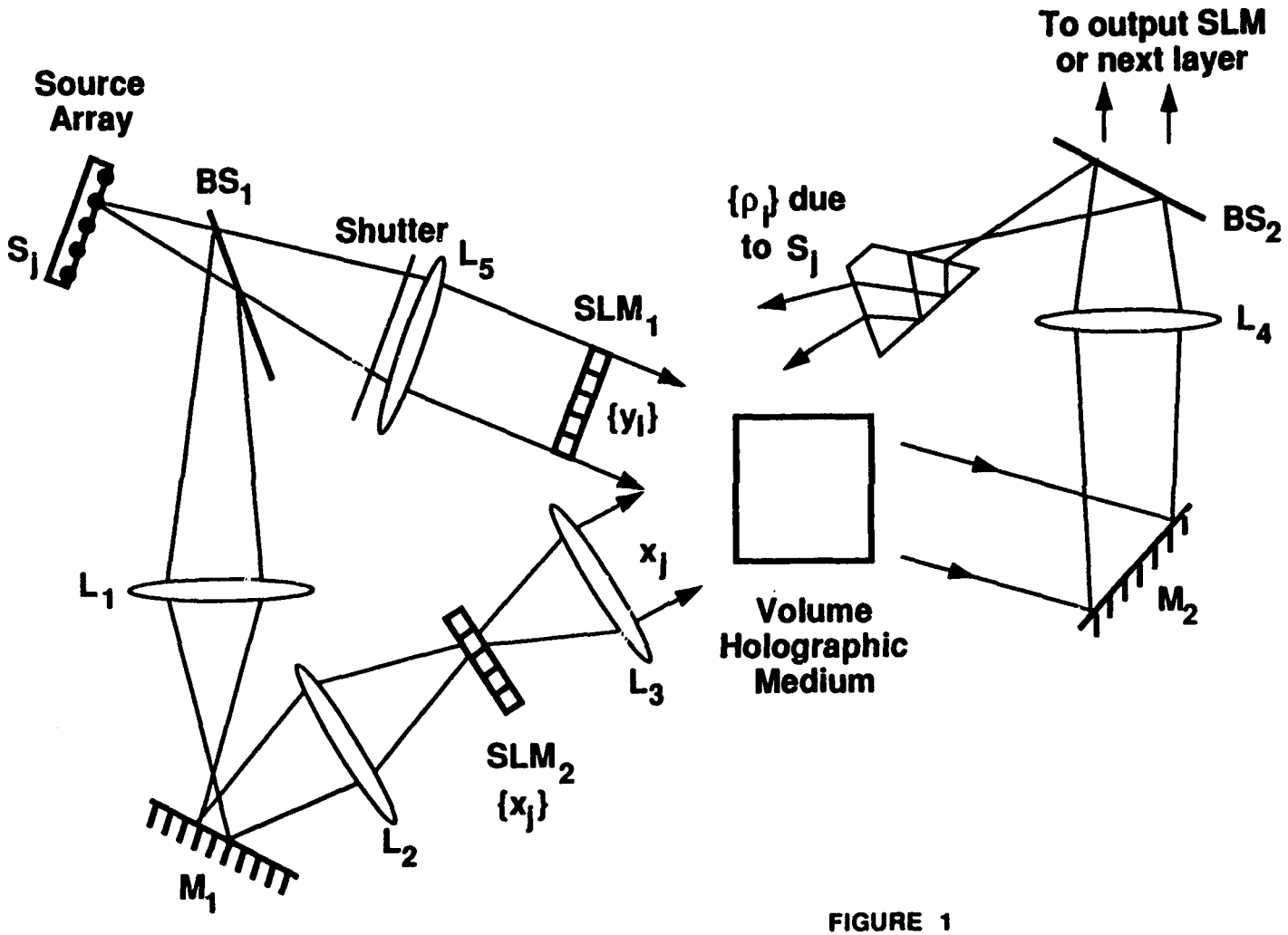

FIGURE 1

Schematic diagram of a generalizable photonic neural network architecture, incorporating incoherent/coherent and double angularly multiplexed holographic interconnections, an array of individually coherent but mutually incoherent sources, and spatial light modulators that contain the neuron unit arrays.

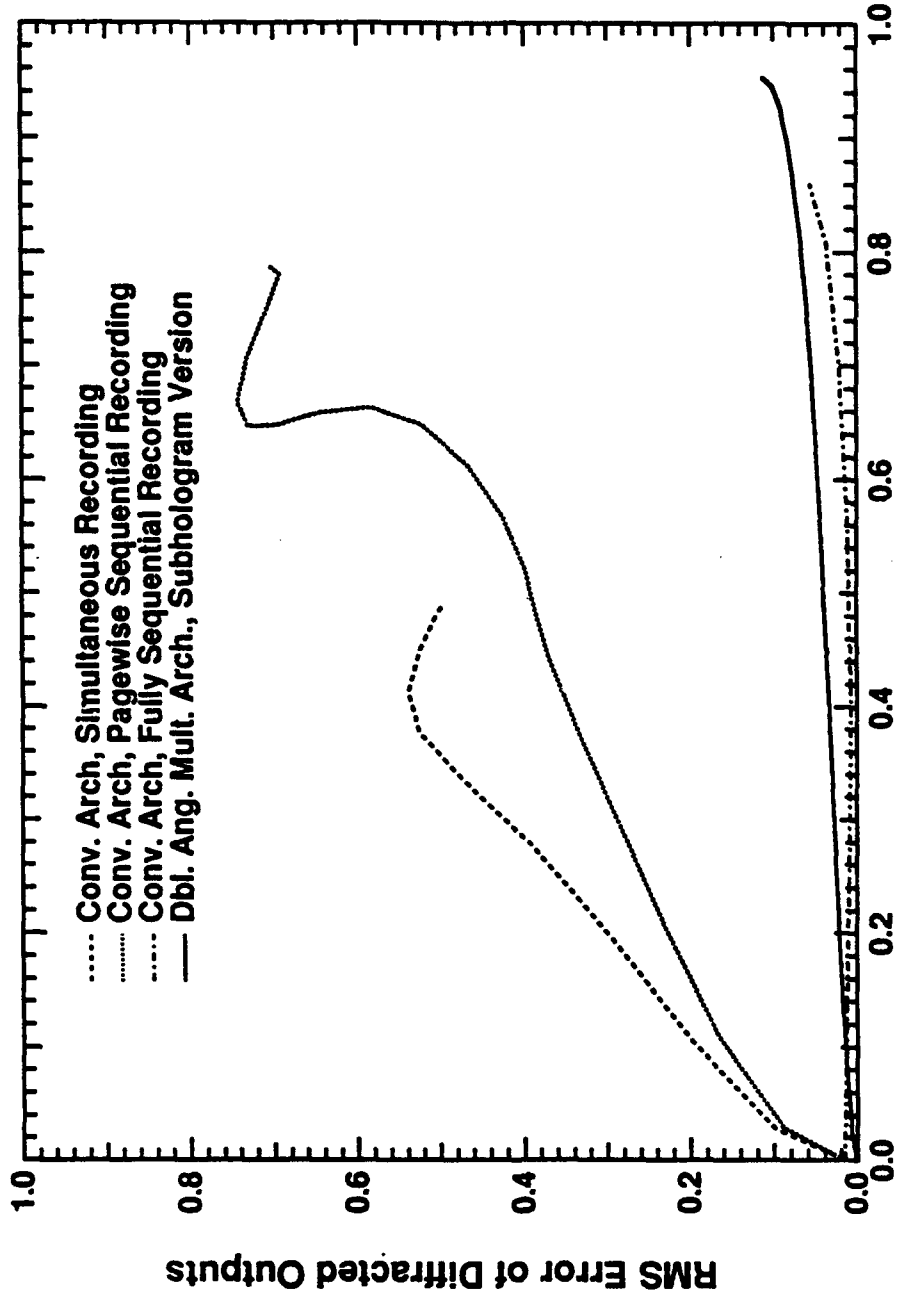

FIGURE 2

RMS error of diffracted outputs as a function of optical throughput for the conventional architecture (using several recording methods) and the subhologram version of the double angularly multiplexed architecture. Beam ratios of 100:1 are assumed for both the conventional architecture using the page-wise sequential recording method and the subhologram version of the double angularly multiplexed architecture.

Strained GaAs/InGaAs/AlGaAs MQW based Modulators for Generalizable Photonic Neural Networks and Digital Optical Switches for Optical Interconnects

A. Madhukar

OVERVIEW: During the reporting period of this final technical report, A. Madhukar's commitments were to develop III-V multiple quantum well (MQW) based spatial light modulators that may provide the neuron-like functionality needed for the project "Generalizable Photonic Neural Networks" proposed jointly by B. K. Jenkins, A. Madhukar, and A. R. Tanguay Jr. To this end, three lines of investigations were proposed: (i) development of the physics, growth, processing, and characterization of GaAs(001) substrate/InGaAs/AlGaAs MQW based asymmetric Fabry-Perot modulator arrays involving post-growth photolithographic pixellation with pixel linear size ~150μm. (ii) Exploring post-growth patterning employing focused ion-beam *in-situ* etching on submicron length scales as a possible means of realizing lateral confinement of the optical excitations. (iii) Growth on substrates pre-patterned via photolithography on ~20μm length scale. Considerable work on (ii) was undertaken during the first year to establish the limits of the FIB spatial patterning length scale achievable in the vibrational environment of the laboratory on the fifth floor of the building. It was found to be ~1.5μm. It was expected that the experimental facility will be moved to solid ground to allow full use of the FIB capability (800°A) and avoid the expected vibrational limitations but regrettably this did not happen. As a result, starting from the second year, this effort was replaced by a focus on the use of modulator structures in digital optical switches for optical interconnects - a project which had considerable synergism with other efforts within the Center. In the following we provide a brief summary of the salient accomplishments.

SALIENT ACCOMPLISHMENTS:

1. First Realization of GaAs(100)/InGaAs/AlGaAs *Inverted*-Geometry ASFP Modulators:

Exploiting the transparency of the semi-insulating GaAs(001) substrates to the operational wavelengths provided by the strained InGaAs(well)/AlGaAs(barrier) quantum wells, we focused our modulator efforts on a novel *inverted* geometry asymmetric Fabry-Perot design in which the light is incident through the (antireflectoin coated) GaAs(001) substrate. The first grown GaAs/AlAs Bragg mirror is then a low reflectivity (~65%) mirror involving only 5 to 6 periods of GaAs/AlAs quarter wave stack (rather than the high reflectivity, ≥99%, Bragg mirrors requiring ~20 periods to be grown in the conventional geometry). This also eases considerably the stringent requirements on absolute thickness control which has been one of the limitations in achieving reproducible results in devices involving Bragg mirrors. After the growth of the strained InGaAs/AlGaAs MQW of individual layer thicknesses, compositions, and periods determined via the extensive modeling efforts undertaken, the high reflectivity mirror can be an externally deposited Au mirror (for test purposes) or a quarter wave stack of dielectrics (such as MgF_2/Sb_2S_3 developed in A. R. Tanguay's group) which can provide reflectivity's >99% within 2 or 3 periods due to the greater difference in the refractive indices of the two materials involved in the mirror. Finally, the inverted

geometry is critical to the use of Si electronics based detectors and control logic in a unique, face-to-face, flip chip bonding approach to realizing the needed neuron-like functionality's.

Such inverted geometry reflection modulators were demonstrated for the first time. Initial efforts using InGaAs/GaAs MQWs gave a typical contrast ratio of 12:1 at the FP wavelength (0.95μm to 0.96μm) for an applied bias of about -16V. The efforts subsequently focused on simultaneously achieving (a) reduction in operating voltage near -12V, (b) extending operating wavelength to 0.98μm, (c) contrast ratio > 15:1 for a bandwidth of 50°A, (d) reflectivity change of ~50% for an on-state reflectivity > 50% (i.e. insertion loss less than 3dB), and (e) sufficient uniformity in layer thickness and composition (better than 0.5%) over a sufficient growth area to enable realization of greater than 10x10 arrays with individual pixel size ~30μm. Figure one shows the typical behavior of a modulator pixel in a 15x15 array obtained using, for test purposes, Au mirror with a reflectivity of only 94.6%. As the design of the modulator is based upon >99% dielectric mirror, the actual characteristics are expected to be significantly better than seen in fig. 1.

2. Realization of the first vertically integrated p-i(MQW)-n modulator and heterojunction phototransistor to obtain optically controlled SLM:

While continuing our work on the electrically addressable SLMs, we also examined several options for realizing optically controlled modulators and implemented a design based on vertically integrated emitter-down heterojunction phototransistor and P-i(MQW)-n *inverted* cavity modulator (Fig.2a). The modulator reflectivity at zero and 0.3mW input light power are shown in Fig. 2b. A contrast ratio of 12:1 with a reflectivity change of 27% at the Fabry-Perot wavelength of 9708Å is observed. Work on improved device performance and on extending the operating wavelength to 0.98 μm (through increased In content in the InGaAs / GaAs MQW) can easily be carried out if other systems considerations were to indicate that HPT-SLM integration is desirable for a particular application.

3. ASFP-SLM based digital optical switches:

The p-i(MQW)-n configuration ASFP modulator structures grown were examined for their performance in a wide variety of digital optical switches. Particular emphasis was laid on the use of *inverted* cavity design which permits the read and write light beams to impinge from opposite sides, thus reducing many growth / regrowth and processing considerations otherwise arising the need for optical isolation. The following types of switches were implemented;

(a) Self electro-optic effect device (SEEDs) based on *blue-shift* of the *inverted* cavity ASFP modulator Fabry-Perot Mode:

As opposed to the conventional usage of the exciton red-shift, we implemented a new class of SEED device based upon the *blue shift* of the Fabry-Perot mode in "normally-off" InGaAs / GaAs ASFP modulators. The SEEDs examined included diode-SEED, transistor-SEED, phototransistor-SEED, and the symmetric -SEED. While the details of the first three can be found in publications, we note here the behavior of the symmetric-SEED only. A contrast ratio of 5:1 was realized in the

strained InGaAs /GaAs system comparable to the best GaAs / AlGaAs based symmetric-SEEDs. Details are given in the publications.

(b) Monolithic Opto-Electronic Transistor (MOET):

The MOET is based upon the usage of the negative differential resistance (NDR) of a resonant tunneling diode (RTD) to achieve bistability. A schematic of the circuit is shown in Fig. 3a. The InGaAs / GaAs MQW based p-i(MQW)-n ASFP modulator /detector pixels of the structures grown as part of the effort under item 1 above were thus combined with InGaAs /AlAs / GaAs based RTD's grown under the JSEP program to examine MOET performance. For amplification of the RTD signal, different types of FETs were used. While the details of these different implementation may be found in the publications, here we show in Fig.3b the MOET characteristics obtained when a GaAs MESFET, (grown fabricated, and tested under the sponsorship of JSEP) is used in the circuit. A contrast ratio of 4.5:1 and a reflectivity change of 35% with a fan-out of 2 is obtained. The inherent contrast of the modulator is significantly higher (~20:1) at the 0.8mW bias light power employed when ~15V reverse bias is applied. The lower value of 4.5:1 obtained for the MOET is due to the fact that GaAs MESFET used had a 12V source-drain breakdown voltage and could therefore provide a maximum of ~12V drop across the modulator pixel. The further developments on the modulator front leading to the reduced (~12V) reverse bias needed to achieve >10:1 contrast ratio (see fig. 1) shows that using these modulators, MOETs with improved characteristics are eminently feasible.

4. Defect Reduction via Growth on Pre-Patterned Substrates:

The occurrence of defects such as threading dislocations in strained multiple wells beyond the so-called critical thickness and their deleterious effect on optical and electrical characteristics is a well known problem for applications, such as the modulators of interest here, requiring reasonably thick (~1μm) MQW structures. Although extensive high resolution transmission electron microscope studies carried out by us on our InGaAs/AlGaAs MQWs of thicknesses ranging from 0.8μm to 1.3μm showed that, through our unique approach of optimizing the MBE growth kinetics using RHEED, we were able to create metastable MQW structures that confine the defects to a few (~3) quantum wells near the interfaces with the Bragg mirrors, we nevertheless explored the possibility of eliminating threading dislocations altogether via the approach of growth on pre-patterned mesas introduced earlier by us. We demonstrated for the first time the occurrence (if at all) of threading and misfit dislocations in $In_{0.2}Ga_{0.8}As/GaAs$ MQWs of thickness as large as 2.38μm at a level below the high resolution TEM limit (10^3/cm). To further examine the correlation with the absorption characteristics, collaborative studies with Prof. D. Rich (Materials Science, USC) were undertaken using spatially- and spectrally-resolved cathodoluminescence. These studies have provided the first evidence of a Cotterel atmosphere of point defects that presumably is associated with the dislocation motion to the edges of the mesa.

5. Modulator Speed:

Although it was not a part of the original commitment, once the possibility of the use of the inverted ASFP modulators in digital optical switches was added to the agenda, examining the time response of these modulators became of significance and

interest. As a result, collaborative work was undertaken with Prof. Elsa Garmire to examine the time response using pico-second time-resolved electro-absorption studies. These studies showed that the response time of our modulators is ~6 to 10ps and is limited by the time-of-flight of the excitons across the MQW. Based upon these measurements we calculate that the intrinsic 3dB response of our modulator/detector pixels of size 30μm x 30μm is about 30GH_Z for an optical input power of a few μW per pixel. A carrier sweep-out time of ~10ps corresponds to a transit time limited bandwidth of ~15GH_Z.

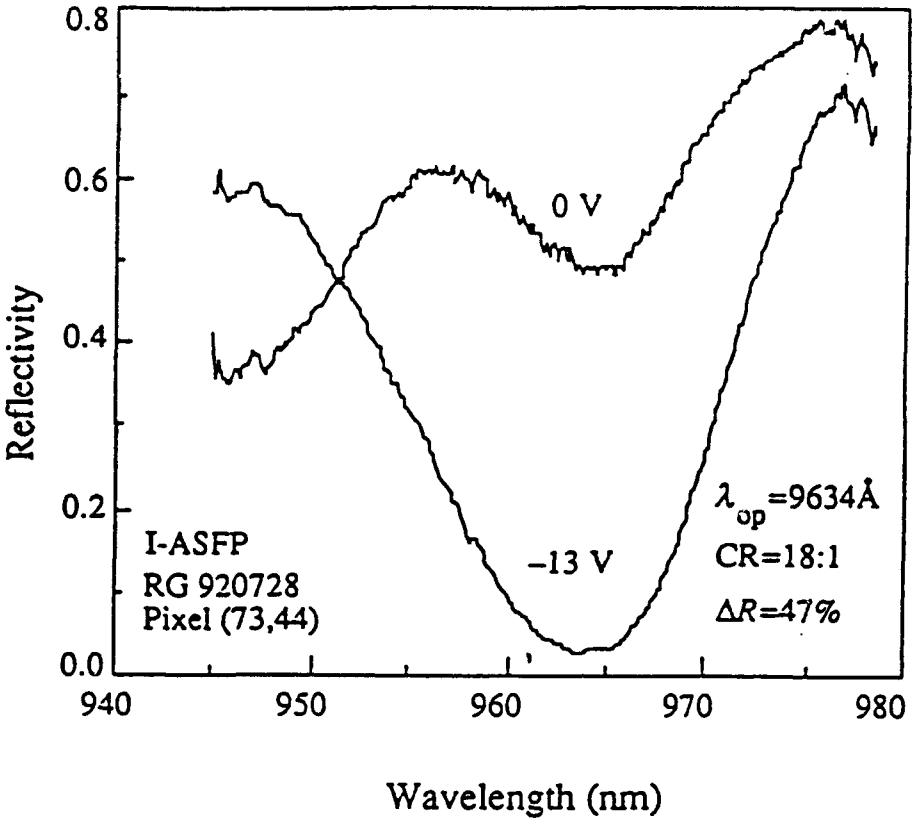

Fig. 1 Measured reflectivity spectra at two biases for I-ASFP modulator RG920728.

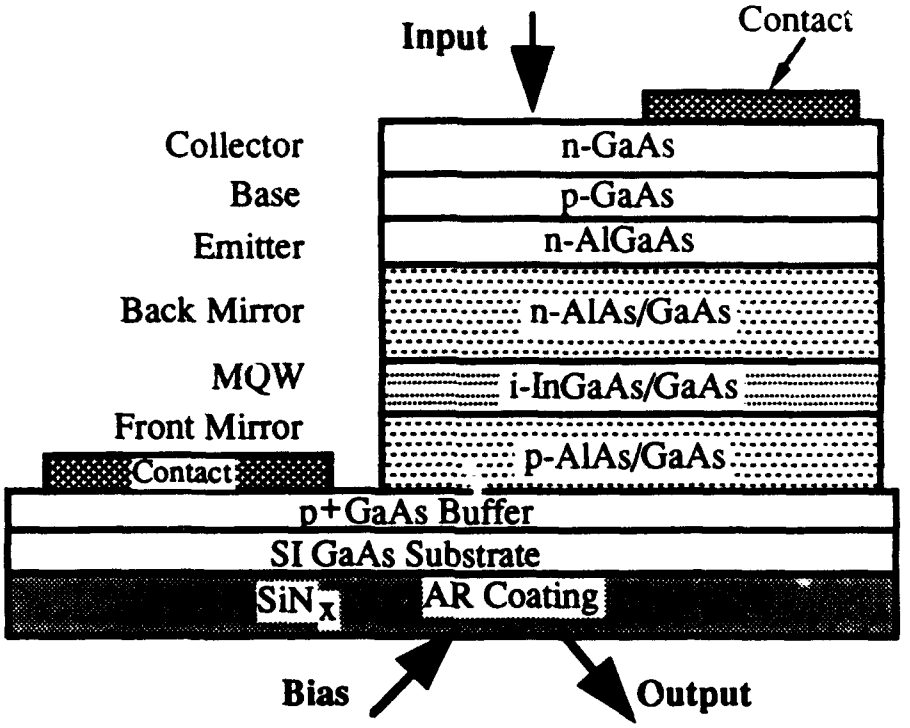

Figure 2a

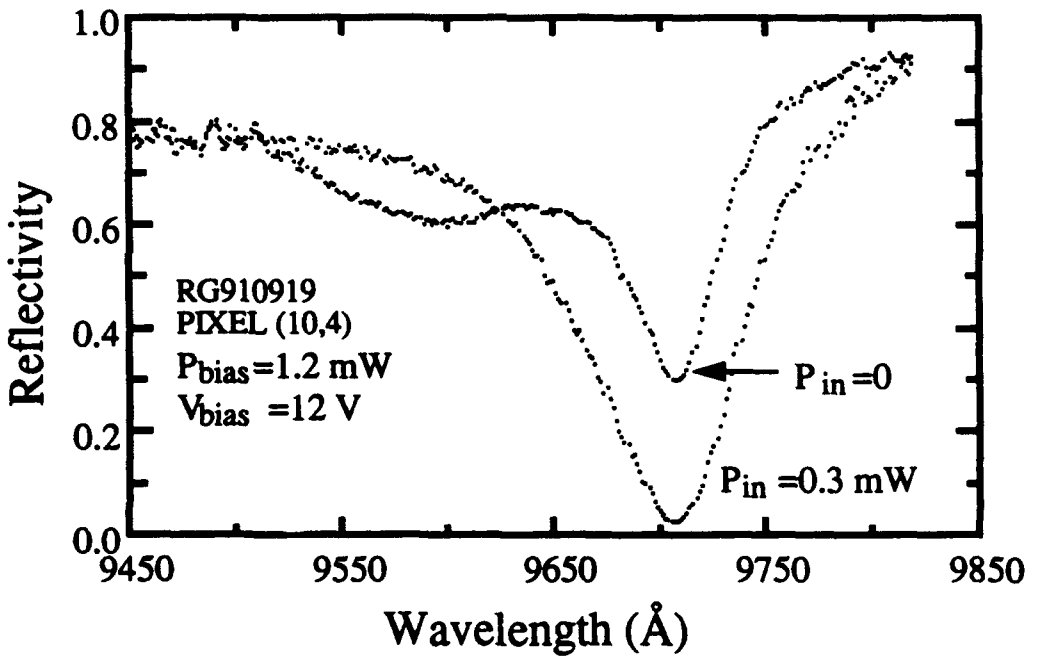

Figure 2b

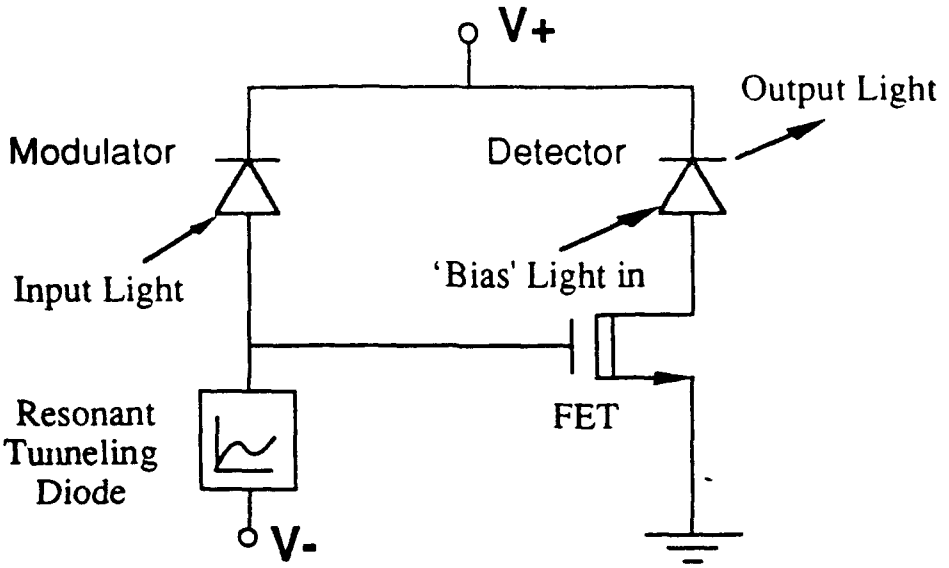

Figure 3a

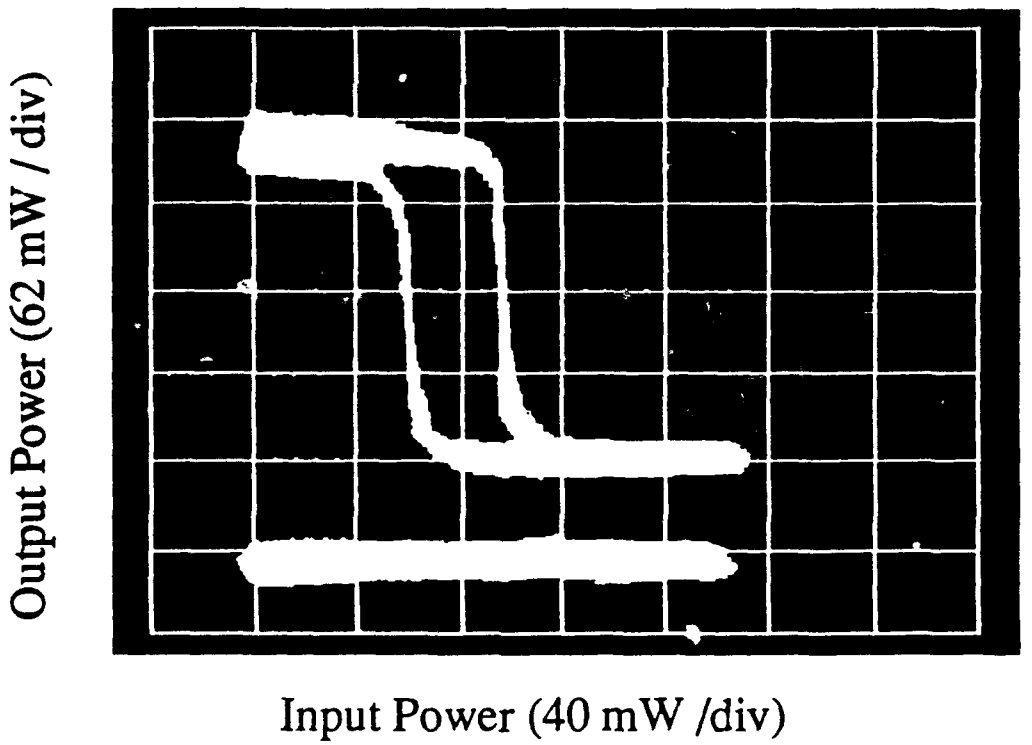

Figure 3b

Applications and Manufacturability of Adaptive Analog Optical Interconnection Systems

B. Keith Jenkins

Work on this grant has included a demonstration of selected applications of a dynamic lenslet array processor that uses a spatial light modulator and a two-dimensional lenslet array as the key elements in an incoherent optical interconnection system. Both fixed and adaptive interconnections were experimentally demonstrated, and included digital circuits as well as binary and analog neural networks.. In addition, the lenslet array processor system was characterized in detail.

In parallel with our efforts on adaptive photonic neural networks, we have developed and demonstrated under this grant the single-step copying of multiplexed volume holographic optical interconnection elements. This copying technique utilizes a set of individually coherent but mutually incoherent optical sources. We have demonstrated the concept experimentally for the case of three angularly multiplexed holograms that are spatially coincident on a dichromated gelatin or photopolymer plate.

The remainder of this section describes these efforts in more detail.

A lenslet array processor (LAP) can implement both neural networks and digital logic circuits using a hybrid optical and electronic system. As shown in Fig. 1, the system incorporates optical interconnections using a lenslet array, an input (electrical to optical) spatial light modulator, a dynamic interconnection mask implemented via another spatial light modulator, and an output device (CCD for optical to electronic conversion). A computer is included in the loop to operated on optical system outputs, to generate optical system inputs for the next iteration, and to control the interconnection pattern.

In cooperation with A. A. Sawchuk of the URI center, the system has been demonstrated in our laboratory under this URI program at the level of a 4 x 4 input array of 16 neurons, with up to 256 interconnection weights per layer. We have demonstrated a number of working system applications, in two waves. The first wave of experiments demonstrated binary, fixed-interconnection systems. The second wave of experiments demonstrated analog and adaptive systems.

The binary, fixed-interconnection systems that were demonstrated included a unipolar neural network solving the 3-bit parity problem, a unipolar neural network implementing a simple associative memory, and a digital logic circuit implementing a 3-to-8 decoder. All three systems functioned correctly. While each system utilized a fixed interconnection, the hardware incorporates a video CRT and liquid crystal light valve for implementation of the interconnection weight mask, so that it is compatible with adaptive networks or reconfigurable interconnections in a digital circuit.

Several experiments demonstrated the capability for analog signals, adaptive neural networks, and bipolar (both positive and negative) signals. A well-known pattern recognition classifier algorithm, a multiclass perceptron, was implemented on

the LAP. This was implemented as a neural network that is trained for a particular set of pattern classes. Different input spatial patterns, each comprising a 4 X 4 array of pixels, were grouped into classes and used to train the network. Both two-class spatially invariant, and four and five class problems, were successfully demonstrated.

A second adaptive neural network experiment was competitive learning. Competitive learning is an unsupervised learning algorithm in which the neural network decides on which input patterns are grouped into which classes. Such networks are useful, for example, in feature extraction. This experiment was performed as a two-layer neural network (i.e., one hidden layer of neuron units), and used analog-valued input patterns.

A very common and useful operation in neural networks, pattern recognition algorithms, and some associative memories, is that of maximum finding. Maximum finding (of analog-valued inputs) is a non-trivial operation to perform in a neural network. Two different types of maximum finding networks were implemented. The first and more straight forward such network was a lateral inhibition network, or on-center off-surround network. It performed, in optics, as the ideal neural network model predicted. This result indicates the capability of the optical LAP system, but the maximum finding performance is limited by the neural network model being implemented. The more sophisticated and better performing maximum finding network that we implemented was the Didday prey selection model, and is based on a leaky integrator neuron unit model. It performed well, and in fact the optical system typically converged in fewer steps than was predicted by simulation of the neural network model.

The LAP system, as implemented, can provide useful information on the viability of different optical or optoelectronic device responses and imperfections when used in an optically interconnected system, by programming the appropriate characteristics into the computer software.

We have also, under this grant, performed preliminary design and evaluation of an integrated optoelectronic LAP system. Issues such as communication bottlenecks, and system volume and device area minimization, have been addressed. These issues indicate that an integrated LAP system is feasible, but that substantial electronic integration is required in each pixel of an optoelectronic smart-pixel spatial light modulator (SLM) in order to provide a small, integrated implementation. This result further implies that the use of hybrid integration of silicon electronics with optical liquid crystal or III-V-based modulators is appropriate for a near term implementation, while for the case of a longer term implementation using monolithic GaAs-based devices, further progress in GaAs electronic integration densities and capabilities are needed. Work on hybrid integrated silicon/GaAs smart pixel SLMs employing analog silicon electronics for neuron unit function, silicon detection for optical input, and III-V based modulation for optical output, has been underway by Armand R. Tanguay, Jr., and Anupam Madhukar, both of the URI Center.

Under a separately funded effort that was spawned out of seed work performed under our previous URI grant, we have been developing a class of volume-hologram based photonic architectures for the implementation of generalizable neural networks.

This is a joint project that is performed in conjunction with Prof. Armand R. Tanguay, Jr. and Prof. Anupam Madhukar, both of the URI Center. The basic architectural concept utilizes an array of coherent but mutually incoherent sources to write and recall interconnection patterns that are stored in a volume holographic medium. This optical interconnection system can also be applied (with some modification) to other systems, including digital computing interconnections and wavelength division multiplexed telecommunications switching systems. A key question becomes the manufacturability of these multiplexed volume holographic elements, whether used for interconnections or for holographic optical elements. Toward this end, we have developed, under the current URI grant, a technique for rapidly copying such a multiplexed volume holographic element.

Along these lines, we have demonstrated, to our knowledge for the first time, the single step copying of a multiplexed holographic optical element. The copying technique can be applied directly to the copying of a set of neural weighted interconnections. In the copying process, an array of individually coherent but mutually incoherent laser sources provides a set of reference beams that recall all of the stored holograms in a *master* holographic medium, and a duplicate path sends the set of reference beams to a *copy* holographic medium. The object beams recalled from the master hologram are also sent to the copy holographic medium; each object beam interferes with the corresponding reference beam, making a complete copy in one step. We have successfully demonstrated the copying of 3 multiplexed holograms (each of which is an independent volume grating) in dichromated gelatin, done in a single simultaneous exposure. Analyses of some of the potential and limitations of this copying technique have also been performed. In addition, it can potentially be used to copy general classes of holographic optical elements.

Figure 2 shows the architecture that provides for single-step copying. A set of individually coherent but mutually incoherent sources is used to generate a set of reference beams. Each such beam is intended to duplicate, at the master holographic element, the angle, location, and phasefront of the corresponding reference beam that was used to expose the master holographic element. For cases in which the reference beams are incident in a regular angularly multiplexed geometry, a regular 1-D or 2-D spatial array of sources can generate the beams. Such an array of mutually incoherent sources can be either fabricated or generated from a single coherent source and an optical system. In the architecture shown, the reference beams illuminate the primary (master) holographic element simultaneously, recalling all of the stored holograms in parallel. The source array is imaged so that it generates a set of individually identical reference beam phasefronts on the secondary (copy) holographic medium. In Fig. 2, the reference beam phasefronts in planes P_1 and P_2 are identical. Similarly, the reconstructed object beams are also imaged in amplitude and phase onto the secondary medium. The appropriate pairs of beams interfere in the secondary holographic medium, making a complete copy of the original multiplexed hologram.

Note two aspects of this copying technique. First, it is the mutual incoherence of sources that permits the copy process to be performed in a single exposure step. Second, the relative phases among the different holograms can in principle also be preserved in the copy by using a sufficiently stable and aberration-free optical system.

However, in this report we consider only systems and applications in which these relative phases are not of concern.

In several preliminary demonstrations of this concept, a master holographic element was used that consisted of three angularly multiplexed volume holograms, superimposed onto a region of a holographic plate. We have performed these experiments in both dichromated gelatin and DuPont photopolymer materials.

In the copying architecture, a set of individually coherent but mutually incoherent reference beams illuminates the master holographic element. Each reference beam has the same incident geometry as the reference beam used during recording of the master holographic element. The three illuminating reference beams then result in the reconstruction of the three object beams. A three lens system images the amplitude and phasefront of each reconstructed object beam onto the copy holographic medium. Beamsplitters provide duplicates of the master reference beams at the copy holographic medium; the optical path lengths are kept equal, pairwise, to insure mutual coherence between each object beam and its corresponding reference beam at the copy.

In all cases, the copy was made in a single step exposure. Measurements reveal negligible crosstalk between the different multiplexed holograms in the copy holographic element. Simple holograms that map plane waves to plane waves (common in interconnection systems), and complex holograms of spatial objects, have been successfully copied.

We have performed an initial analysis of some of the potential and limitations of such a copying system. In addition, extensions of the copying system to allow for the generation of non-identical copies are also possible. For example, additional holograms can be added in conjunction with those copied from the master; the nature of the reference beams at the copy can be different from those of the master if desired; in some cases filtering can be performed on the object beam path from the master to the copy to decrease noise; magnification can potentially be inserted between the master and the copy; and the relative diffraction efficiencies can be changed by altering either each beam-pair ratio or each beam intensity.

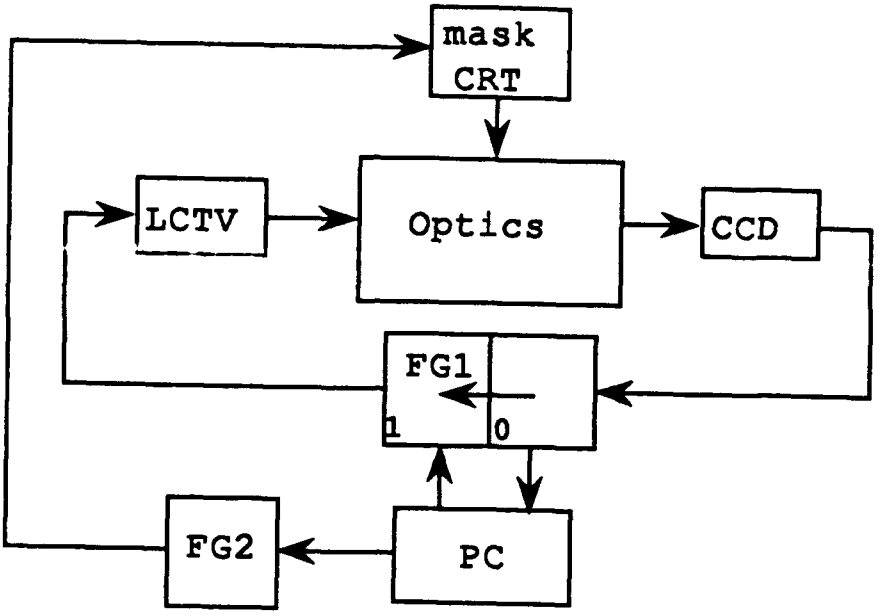

(a)

Figure 1 Lenslet array processor.

(a) Entire system. Data flows through the optical interconnection from left to right; the control information (interconnection pattern, routing, or learning updates) enters from above. The personal computer (PC) implements the gate or neuron nonlinearity, summing and differencing via frame grabber boards (FG).

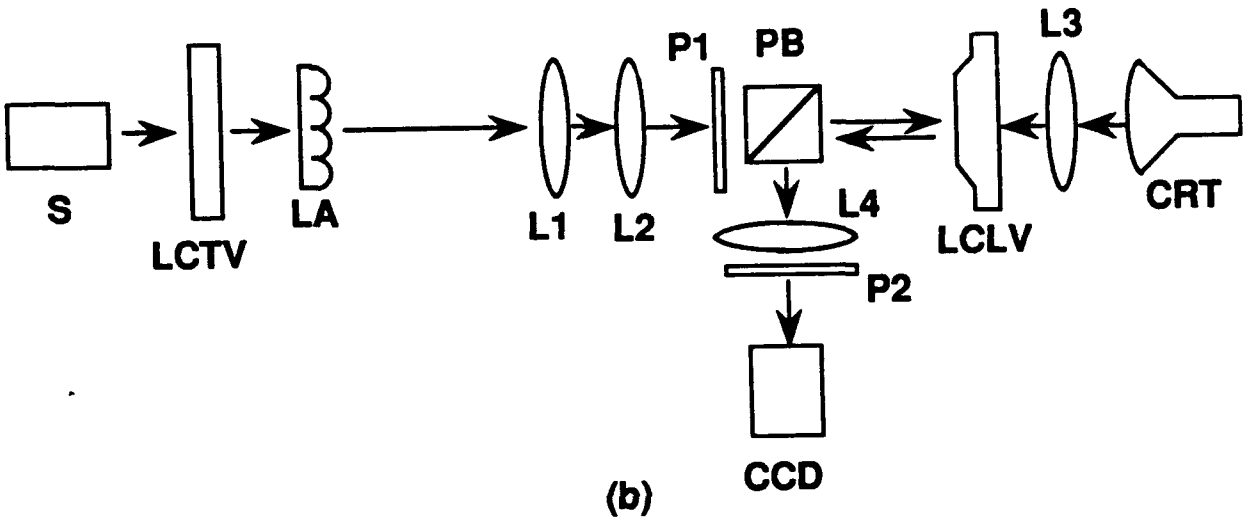

(b) Optical subsystem of experimental lenslet array processor (LAP). S: incoherent source, LCTV: liquid crystal television (interconnection input), LA: lenslet array, P1,2: polarizers, PB: polarizing beamsplitter, LCLV: liquid crystal light valve (programmable interconnection mask).

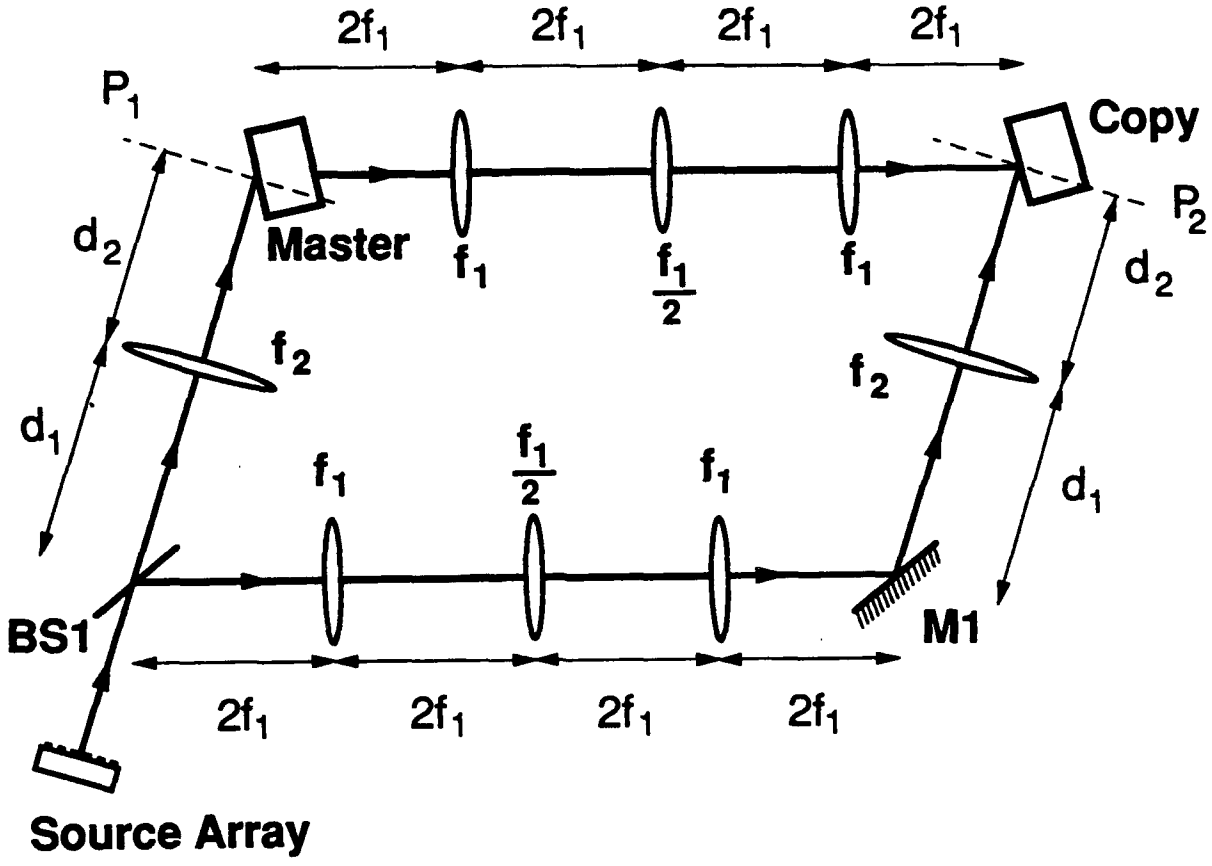

Figure 2.

Optical system for single-step copying of a multiplexed volume holographic element. M: Mirror, BS: Beam Splitter.

Ultralow Threshold Laser Array Elements

P. Daniel Dapkus

The objective of this program has been the investigation of device designs and technology for the fabrication of ultralow threshold, high efficiency surface emitting laser (SEL) arrays that can be incorporated into linear and areal arrays and into smart pixels. These objectives are considered to be of paramount importance to the practical realization of interconnections using laser arrays. We have explored the folded cavity surface emitting lasers as an alternative to the widely investigated vertical cavity SEL's[1-2] because of the tradeoff between low threshold current and high efficiency inherent to the VCSEL design. We have also not investigated edge emitting lasers with external deflectors[3-8] or edge second order distributed Bragg reflectors owing to the limitations of both in achieving low threshold and high efficiency. In the course of our work we have 1.) developed in situ monitoring and control techniques for reproducible growth of Bragg Reflectors by MOCVD using laser reflectometry; 2.) developed the temperature engineered growth (TEG) technique for the fabrication of ultralow threshold InGaAs/GaAs/AlGaAs strained layer lasers; and 3.) analyzed and demonstrated a new folded cavity surface emitting laser (FCSEL) that has potential as an emitter in smart pixel arrays.

The ultimate objective of our work has been the FCSEL shown schematically in Fig. 1a. The device consists of stripe geometry horizontal cavity gain region, two internal 45° mirrors to deflect the light to the cavity mirrors that are constructed from high reflectivity Bragg mirrors. Such folded cavity lasers have the advantage of a much longer gain path than VCSEL's that results in less stringent requirements for high reflectivity mirrors. Also with the longer cavity, the FCSEL free spectral range becomes much smaller, which eases the requirements of the Bragg mirror phase response to achieve matching of the gain spectrum to the cavity resonance. As a result, a reduction of the required number of mirror layers and a relaxation of the growth thickness control is obtained. A weaker temperature dependence of the device operation is expected that will result in devices with higher efficiency and higher output power. Finally, more design flexibility is achieved, for example, by allowing the use of material systems with lower range of indices of refraction and by providing the opportunity to incorporate intracavity modulators, tuning elements, and other wave guide components into the cavity.

In this work, we integrated the FCSEL structure with a high reflectivity Bragg reflector for emission towards the substrate with a laser structure fabricated by the temperature engineered growth (TEG)[9-10] of InGaAs/GaAs GRINSCH lasers on structured substrates. As discussed in previous reports, TEG is an efficient and simple technique for growth of laser structures in a single growth with good lateral optical and current confinement. Little post growth processing is needed to fabricate the device potentially resulting in better yield and uniformity. This approach was developed during the first three years of the program. We now exploit it for many device structures including the subject one. The inset in Fig. 1 shows a cross sectional SEM picture along the stripe direction of the device showing one of the 45° deflecting mirrors and the Brag mirrors at one of the edges of the device.

The structures were grown in two steps by MOCVD. First a 9 1/2 pair Bragg reflector with a 88% plane wave reflectivity at 0.98μm was grown. A 4 μm GaAs layer was then grown for patterning the subsequent growth. At this point, the reflectivity spectra was characterized and the overgrown GaAs layer was patterned for the TEG laser structure . The TEG laser growth is performed as described in previous reports resulting in a InGaAs/GaAs GRINSCH buried heterostructure laser with 1.5 to 3 μm wide active regions. TEG lasers without the Bragg reflector layers and with cleaved mirrors were demonstrated with laser thresholds as low as 3 mA and with differential quantum efficiencies as high as 90%. More recently under funding from ARPA we have extended the TEG technique to form lasers with thresholds as low 1 mA uncoated and 250 μA with two high reflection coatings. These devices which are a direct result of the work on this program are among the lowest thresholds ever observed. More important these devices exhibit efficiencies as high as 90%. These characteristics make them ideal digital sources.

The Bragg reflectors were grown on a planar substrate using laser reflectometry[11] to determine the growth rate of the various materials prior to growth of the actual structures. By monitoring the reflection of a 6328Å laser beam from the surface during the deposition of calibration layers at the beginning of the growth run, we are able to determine the deposition rate of GaAs and AlAs for the chosen flows. This is sufficient for us to calibrate all growth rates and compositions for the run. In fact we have developed the software and hardware on this program to accomplish all of these tasks automatically prior to the growth of the actual device structure. The program calculates the pressure (flow rates) of each of the reactants required for the compositions in the desired structure and adjusts the growth time of each layer to achieve the required thickness. Using this automated approach to control of the MOCVD growth we are able to achieve 1% reproducibility of the center wavelength of Bragg reflectors. After the growth of the Bragg structure, the wafer is etched to form the required mesa structures for TEG growth and a conventional edge emitting InGaAs GRINSCH strained layer laser is grown by the TEG process to form a buried heterostructure laser. The wafer is then processed to apply contacts and to fabricate the 45° deflectors.

The LxI plot for a device with 1mm long cavity and 1.5 μm active region width operated cw on a probe station is shown in Fig. 2[12]. The dotted curve shows the measured power output before assuming a 30% reflection on the back of the uncoated substrate. Threshold currents of 8 mA are achieved with a total external efficiency of 10 % for both output windows (13% if the substrate reflection correction is introduced). The lasers exhibit single longitudinal mode emission at 0.99 μm with 7dB side mode suppression when driven at 3 x Ith. A 10 ohms series resistance and a diode turn on of 1.34V allowed the laser to pass 53.3 mA at 2 V resulting in a cw wall plug efficiency of 5 % at 6 mW of laser output power.

In order to investigate the feedback to the guided mode provided by the 45° deflection mirror-Bragg mirror combination, a group of FCSEL lasers were cleaved to result in bars containing devices of various cavity lengths with one cleaved 30% reflective mirror and one 45° deflecting mirror-Bragg mirror combination. The pulsed threshold current is obtained as a function of the cavity length. Using empirical gain

parameters obtained in previous experiments with standard broad area edge emitting lasers of the same material we can model the dependence on length by using the reflection/feedback at the 45° mirror as a variable. In order to best fit the data an internal feedback of 11% is calculated.

To understand these results and to project the potential performance of these devices, we have modeled the interaction of the guided wave with the deflecting mirror and the Bragg reflector[12-13]. In these calculation we have included the beam diffraction and the effects of the propagation of non planar waves in the Bragg reflector. We found that the Bragg reflector reflectivity at 0.99 μm drops from 88 % to 84 % as a result of the non planar wave front, and that the divergence of the beam after traveling the 5.76 μm between the 45° deflector and the Bragg reflector and inside the Bragg mirror results in a reflected spot width of 8 μm . The coupling integral between the two distributions is 13 % in reasonable agreement with our experimental result value of 11 %. With these results one can also estimate the expected external efficiency for the FCSEL structure. Assuming an internal loss of 4 cm^{-1}, unity internal efficiency (from the material parameters fitting), a cavity length of 1mm, and a coupling of 13%. the number of photons that escape the guided mode is 83 % of the total number of injected electrons. Of these escaping photons only the photons transmitted through the Bragg reflector are calculated to result in surface emission with the remaining photons not being coupled back to the laser mode nor to the output power. The overall external efficiency then should be 13%. This value matches well efficiency obtained with the correction for substrate reflection. Since no scattering loss due to roughness of the 45° mirror was included in the calculation, we expect it to be small. We also should note that the measured efficiency of the devices depends on the leakage of uncoupled light to the bottom of the substrate and non uniformity of the Bragg reflector growth.

In order to improve the external efficiency of such devices without changing the threshold, a design combining a lower reflectivity Bragg mirror to provide more escape for the photons and positioned closer to the active region to reduce the beam divergence is indicated. For example, if a Bragg mirror with 21% reflectivity had been placed 1 μm away from the active region center for the device presented here, we would expect the threshold to remain the same since there would be no change in the calculated coupling, however, the external efficiency would increase from 13 % to 65 %. One could also reduce the threshold by keeping the 84 % reflectivity Bragg mirror, but positioned closer to the active region center to achieve a much lower beam divergence and higher coupling.

Based on our calculation one can lower the threshold current in these devices by moving the mirror closer to the active region. Fig. 3 shows the calculated threshold current for our device as a function of the separation between the output of the waveguide and the Bragg mirror, z_M. A threshold current limit of 3.3 mA is expected for a device 1mm long with, two 45° deflecting mirrors on the edges, and the $9\frac{1}{2}$ pairs AlAs/GaAs Bragg reflector if the distance from the Bragg mirror to the waveguide center is reduced to zero. One also may improve the external efficiency without compromising considerably the threshold current of such devices by utilizing a design that employs a lower reflectivity Bragg mirror, to provide more escape for the photons,

but positioned closer to the active region to reduce the beam divergence shown. Fig. 3 also shows the calculated threshold current as a function of z_M for a structure employing a Bragg mirror with $3\frac{1}{2}$ AlAs(832Å)/GaAs(702Å) pairs for a 35% plane wave reflectivity. As expected we observe an increase in threshold for a given z_M for the device with lower reflectivity. Finally in Fig. 3 we plot the calculated external efficiency for both devices as a function of z_M. We observe that with z_M=2 μm the device with lower reflectivity Bragg reflector has the same threshold current as our measured device with a 87.5% reflectivity Bragg reflector placed at z_M=5.76 since improved coupling to the cavity is obtained by reducing the beam divergence. Also more importantly, the external efficiency is improved from 13 % to 54 %. The photon escape rate from this cavity is higher and the fields are less divergent, therefore the photons are more efficiently used.

In conclusion, we have developed a novel FCSEL structure that integrates a Bragg reflector with a strained InGaAs/GaAs laser grown on a structured substrate. These devices when optimized will be suitable for use in integrated smart pixel arrays. Threshold currents as low as 8 mA with 5 % wall plug efficiency at 6 mW of DC output power were obtained for devices without an AR coating. We determined experimentally that in this particular structure the coupling provided by the Bragg mirror-45° deflection mirror structure is 11 %. We have developed a method for the calculation of the beam divergence out of the wave guide including the effects of the propagation of non-planar waves through the multilayer Bragg reflectors. The reduction of the reflectivity caused by non-planar wave front propagation has been calculated[13]. Since the method is general, based on the solution of the Helmholtz equation, it can be applied in the design of any optoelectronic device that utilizes the propagation of diverging beams through multilayer structures, such as VCSEL and Bragg reflector Fabret-Perot modulators. Based on our calculations, we show how to improve the threshold current in our devices as well as how to increase the external efficiency without compromising the threshold current.

References

1) R. S. Geels, S. W. Corzine, J. W. Scott, D. B. Young, and L. A. Coldren, *IEEE Photon. Technol. Lett.*, **2**, 234 (1990).

2) B. Tell, K. F.. Brown-Goebeler, R. E. Leibenguth, F. M. Baez, and Y. H. Lee, *Appl. Phys. Lett* **60**, 683 (1992).

3) S. S. Ou, M. Jansen, J. J. Yang, L. J. Mawst, and T. J. Roth, *Appl. Phys. Lett.* , **59**, 2085 (1991).

4) F. R. Gfeller, P. Buchmann, K. Dätwyler, J. P. Reithmaier, P. Vettiger, and D. J. Webb, *IEEE Photon. Technol. Lett.* **4**, 698 (1992).

5) W. D. Goodhue, K. Rauschenbach, C. A. Wang, J. P. Donnelly, R. J. Bailey, and G. D. Johnson, J. of Electron. Mater. **19**, 463 (1990).

6) C. P. Chao, K. K. Law, and L. Merz, *Appl. Phys. Lett.* **59** ,1532 (1991).

7) C. P. Chao, K. K. Law, and J. L. Merz, *IEEE Photon. Technol. Lett.*, **4**, 223 (1992).

8) D. W. Nam, R. G. Waarts, D. F. Welch, D. R. Scifres, *IEEE Photon. Technol. Lett.* **5**, 281 (1993).

9) K. M. Dzurko, E. P. Menu, C. A. Beyler, J. S. Osinski, and P. D. Dapkus, *IEEE J. Quantum Electron.* **25**, 1450 (1989).
10) N. C. Frateschi, J. S. Osinski, C. A. Beyler, P. D Dapkus, *IEEE Photon. Technol. Lett.* **4**, 209 (1992).
11) N.F. Frateschi, S.G. Hummel, P.D. Dapkus, Elec. Lett.**27** 155, (1991).
12) N. C. Frateschi and P. D. Dapkus, S. S. Ou, J. J. Yang, and M. Jansen, *Phtonics tech. Letters* **5**, 738 (1992).
13) N. C. Frateschi and P. D. Dapkus, S. S. Ou, J. J. Yang, and M. Jansen, IEEE J. Quantum Electron. in press.

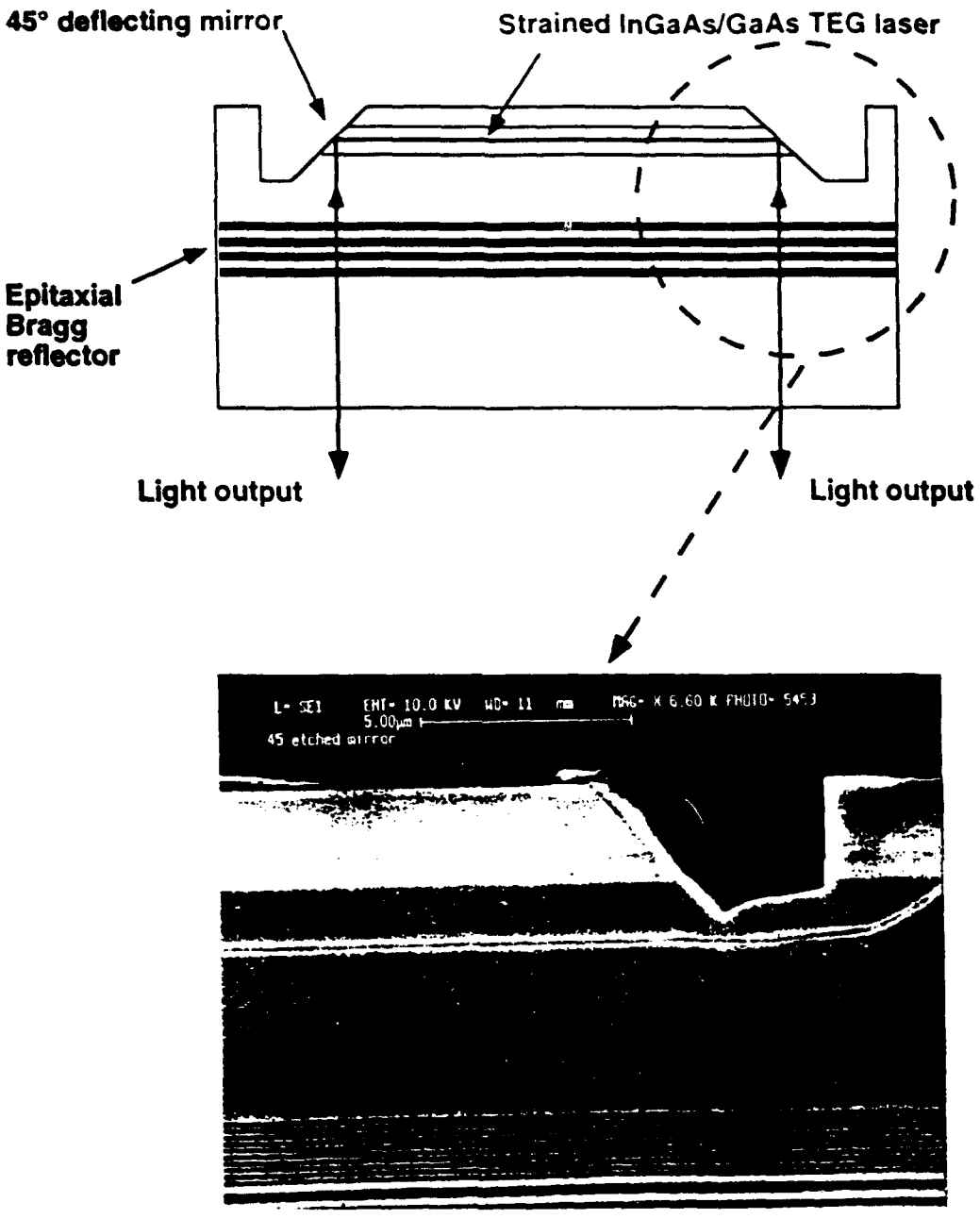

Figure 1

a) Schematic Cross section of FCSEL showing 45° deflecting mirror and Bragg reflector.

b) SEM cross section of the actual device showing these same features.

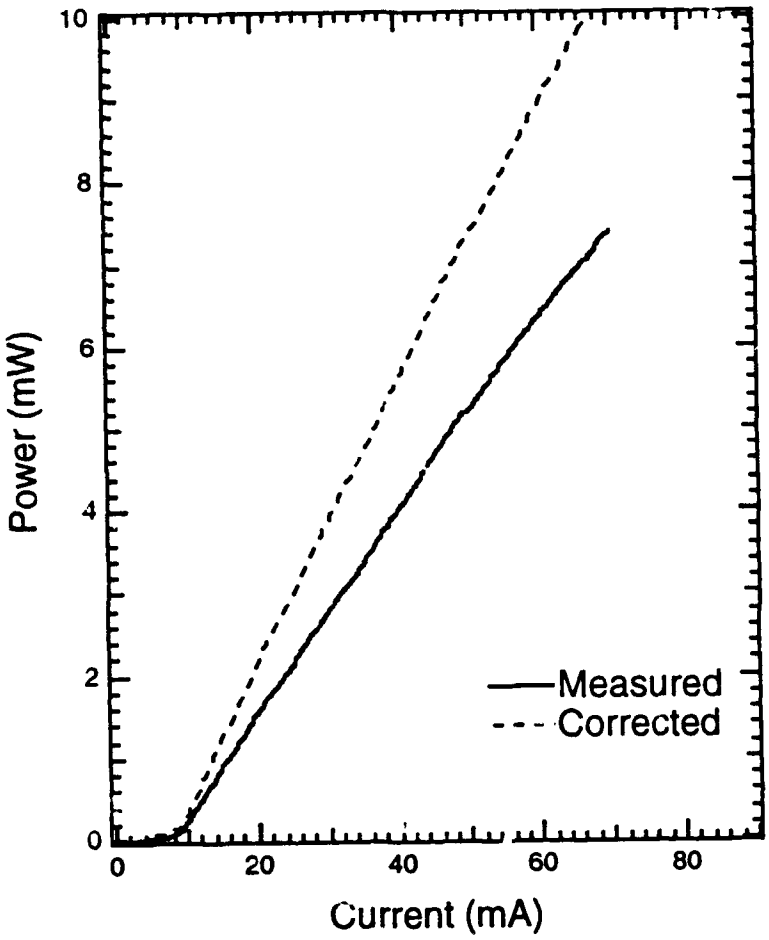

Figure 2

Light output versus current for the FCSEL shown in Figure 1. The dotted curve is shown to indicate the expected output with an antireflection coating on the substrate.

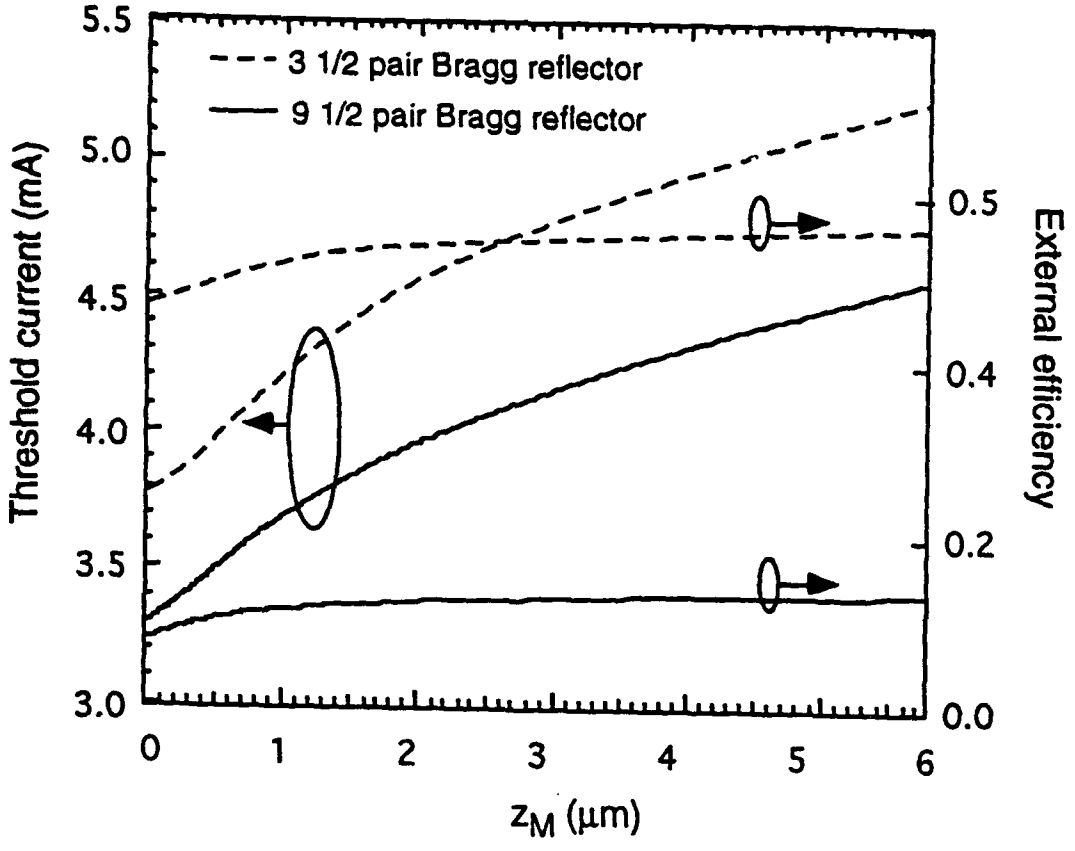

Figure 3

Calculated threshold current and external efficiency for the FCSEL structure as a function of the Bragg mirror distance z_M from the wave guide center for structures with $9\frac{1}{2}$ and $3\frac{1}{2}$ Bragg mirror pairs.

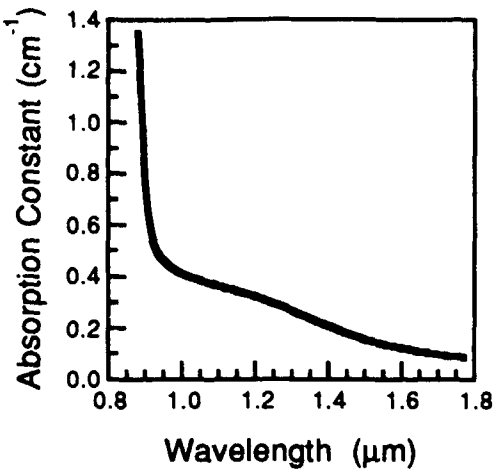

Fig. 1 Absorption spectrum of CdTe:In.

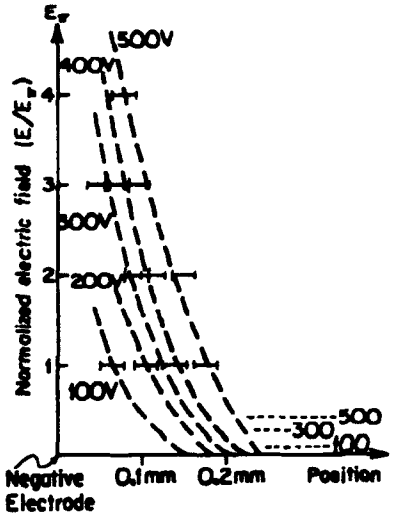

Fig. 2 The mapping of the electric field under the negative electrode for 900 nm illumination. The dashed lines on the side indicate the field value under the ideal uniform conditions.

The formation, persistence in the dark, and the erasure of the high fields can be explained by a rather simple model. The metal-CdTe contact forms a surface barrier that obstructs electron injection from the negative electrode. When negatively biased, the depletion layer of this junction fully extends to the other electrode. The low free carrier density in this high resistivity and heavily compensated material allows a full depletion and a uniform field distribution at moderately low voltages. The effect of light on field profile is through a photoexcitation processes. The below band gap light is absorbed by impurity levels, presumably deep donors, generating electrons that drift away toward the positive electrode and leave behind a positively ionized charged center. The observed high fields are the space charge field that are due to this uncompensated positive charge distribution and the negative charge on the electrode. This charge density is long lived and persist after the end of illumination. The low density of free electrons in the depletion layer and the obstruction of electron injection through the surface barrier are responsible for the scarcity of electrons that can recombine into these centers. The wavelength range that can cause this effect is experimentally found to be in the 850 to 950 nm range.

The electrons that are ultimately able to erase the positive charge distribution in the depletion layer can be optically generated. Illumination through the junction at wavelengths above or very close to the band gap can generate electron-hole pairs near the surface. The holes drift out through the junction while electrons recombine with the positively ionized centers, altogether reducing the space charge and resulting in a field-free region. The penetration depth of light determines the extent of this field free region. This point explains how the 835 nm light creates a broader field-free region while the

780 nm radiation tends to make the field profile uniform across the useful aperture of the crystal.

The electric field distribution in the illuminated plane follows the illumination pattern. We have taken advantage of this property, which is attributed to the high resistivity of the material, for electrooptic device applications. A one-dimensional electrooptic switching array is illustrated in Fig. 3. The principle of operation is similar to a transverse electrooptical polarization modulator where the polarized signal beam is modulated by a longitudinal electric field. By positioning the signal beam close to the negative electrode, one takes advantage of the very high electric fields that are cptically created and erased. The optical control is applied through the transparent top negative electrode, and creates, erases or modulates the high electric field in the vicinity of the negative electrode.

The oscilloscope trace in Fig. 4 demonstrates the principles of the device operation in a latched-type mode. The upper trace represents the control optical pulses at 835 and 900 nm (not to scale). The lower trace is the transmission of a 1.5 μm wavelength signal after the crossed analyzer. The transmitted output (1.5 μm) is initially set low (OFF) by the 835 nm erasure pulse (20 $\mu W/cm^2$) which is followed by the write pulse (7.5 mW/cm^2 @ 900 nm) that sets the transmission high (ON). The transmission stays high (latched) until another erase pulse resets it to low state (OFF). We measured the latching time to be roughly 2 to 5 seconds. Note that both the normally ON and the normally OFF states are available through the choice of the analyzer angle.

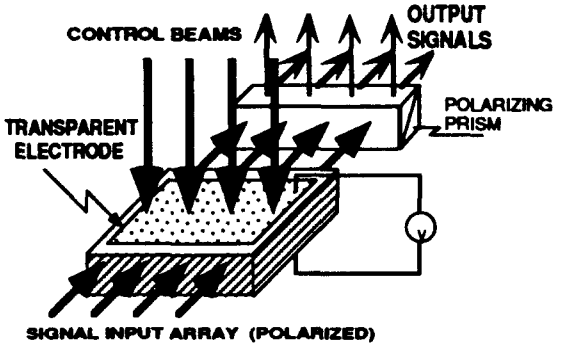

Fig. 3 One-dimensional optically controlled switching array.

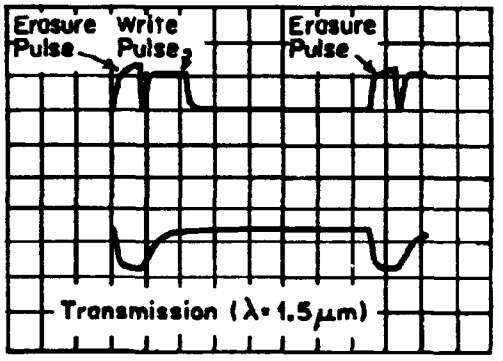

Fig. 4 The latch-type operation of the 1-D switching array. The applied voltage is 100 volts.

The resolution of this array is measured to be roughly 170 line pairs/cm. The contrast in this switching array ranged between 10 to 500 and was affected by the polarizer-analyzer extinction ratio, scattering and the strain-induced birefringence in our samples. The devices operated with a throughput of roughly %50. The absorption loss at 1.5 μm is rather low (~0.65 dB/cm) and the main limit on the throughput was the surface reflections. The erasure energy density (fluence) is 12 nJ/cm^2 which suggest a

switching energy of 12 pJ per pixel considering the minimum device size and our measured resolution. The write energy is similar to that of the erasure, however, it also scales with the absorption constant of the write-wavelength.

An important application issue is the utilization of the field nonuniformity in a 2-D spatial light modulating array where the signal beam propagates along the direction of the applied field. The linear electrooptic effect (Pockels) can not take advantage of the longitudinal light induced field nonuniformity since the net retardation is insensitive to the longitudinal field distribution. The polarization change and spatial modulation of light would need to rely on the transverse component of the electric field. We have used this component for two-dimensional electrooptic spatial light modulation. Our device is very similar to the soviet device known by its acronym PRIZ but has the advantage of offering infrared sensitivity and faster response time.

The large field amplitudes resulting from the field redistribution and the near band-edge sensitivity of this effect can be used in conjunction with the Franz-Keldysh effect for 1-D or 2-D light modulation and switching. We have measured electric field induced positive absorption changes that are comparable to the zero field absorption coefficient. The electroabsorption spectrum extends from the band gap (~830 nm) to as far as 920 nm peaking at around 850 nm.

We have taken advantage of the quadratic nature of electroabsorption such that a longitudinal nonuniform field distribution can result in a net transmission change for a beam that propagates along the direction of the electric field. In this scheme, the applied voltage is a short pulse (~μsec) and the electric field profile depends on the intensity of the incident light.

In summary, we have observed, characterized and modeled an optically controlled electric field distribution in CdTe:In. The findings are important for devices and material studies because a uniform field distribution has fundamental importance for many applications. This effect is observable in other materials and originates from a photo-charge transport process.

B. The Development of Photorefractive Semiconductors and Their Use in Real Time Interconnects

Real time holographic interconnection elements are key to the realization of optical neural networks. In most of the proposed architectures the preferred sources are semiconductor lasers which currently are well developed only in the infrared (0.9 to 1.5mm). In addition, the learning or iteration times for these systems should be on the order of one millisecond or less and the required optical energy should be as small as possible to avoid thermal problems. All of these requirements point to the use of photorefractive semiconductors as the real time holographic media. The semiconductors (CdTe, GaAs, InP) are sensitive in the IR, have photorefractive response times of tens of microseconds, and one of them (CdTe) has the highest measured photorefractive sensitivity(index change per absorbed photon) of any material. Based on this we have made a systematic study of the semiconductors, measuring their photorefractive properties, calculating the possible interconnect

capacities, and collaborating with industry(Brimrose Corp. and Hughes Research Laboratories) to help make available large high quality crystals.

Development of CdTe, $Cd_{(1-x)}Zn_xTe$ and ZnTe Photorefractive Semiconductors

We have completed a basic study of CdTe, ZnTe, and the mixed crystals $Cd_{(1-x)}Zn_xTe$. CdTe has a band gap near 0.9mm and has possible photorefractivity from 0.9μm out to 1.8μm. ZnTe has a band gap near 0.6mm and therefore has potential photorefractivity from the visible into the infrared. By varying the Cd, Zn mixture, a crystal can be grown with a band gap anywhere over the 0.9 to 0.6μm range and potential photorefractivity or other band edge effects over a wide range of wavelengths.

The CdTe is vanadium doped for charge compensation to provide high resistivity material(10^{10}W-cm) and to be a possible source of deep level traps for photorefractivity. Wave mixing gain measurements showed an effective trap density of $2x10^{15}cm^{-3}$ and xr_{41} = 4.4pm/V, where r_{41} is the electrooptic coefficient and x is the electron-hole competition factor. Two beam coupling was measured at 1.06μm, 1.3μm, and 1.52μm. Typical maximum gains of $0.6cm^{-1}$ were observed near 1mm grating spacing and are shown in Figure 5. The equivalent dark irradiance was $88mW/cm^2$ and consequently a mt product in the 10^{-6}-10^{-5} range. The measured index change per absorbed energy per volume was $0.51cm^3/J$; at least an order of magnitude larger than any other material. At an intensity of $10W/cm^2$ the response time was a few microseconds.

We have measured the photorefractivity of vanadium-doped ZnTe in the 630 to 1300 nm wavelength range. There is an ongoing need for improved photorefractive materials at diode laser wavelengths in the 800-900 nm region for several applications. Cubic and ferroelectric oxides lack the required fast and efficient response at these wavelengths while the semiconductors such as CdTe and GaAs have their operating wavelengths limited to greater than 900 nm. We have now shown that ZnTe is a very efficient photorefractive material to fill this need. Two wave mixing gain measurements at 630 nm show a maximum gain of 0.45 cm^{-1} at a fringe spacing of 2 μm. From these measurements a trap density of $1.4x10^{14}cm^{-3}$ and xr_{41} = 4.17 pm/V were derived. This is a relatively low trap density in comparison to other semiconductors($5x10^{15}cm^{-3}$) and suggests that by altering the growth slightly, larger trap densities and gains up to $1.2cm^{-1}$ may be possible. The fastest grating formation time we observed was 14.7 used at 4.7 W/cm^2 which is comparable to GaAs and confirms ZnTe as a fast red-NIR photorefractive material.

We have undertaken the study of photorefractivity in II-VI alloys of CdTe and observed beam coupling gain at 1.318 μm in $Cd_{0.94}Zn_{0.06}Te$:V samples. To the best of our knowledge this is the first observation in ternary II-VI compounds. The bulk alloying capability can lead to the development of materials whose band gap and sensitivity range can overlap the wavelength of application. The measured resistivity

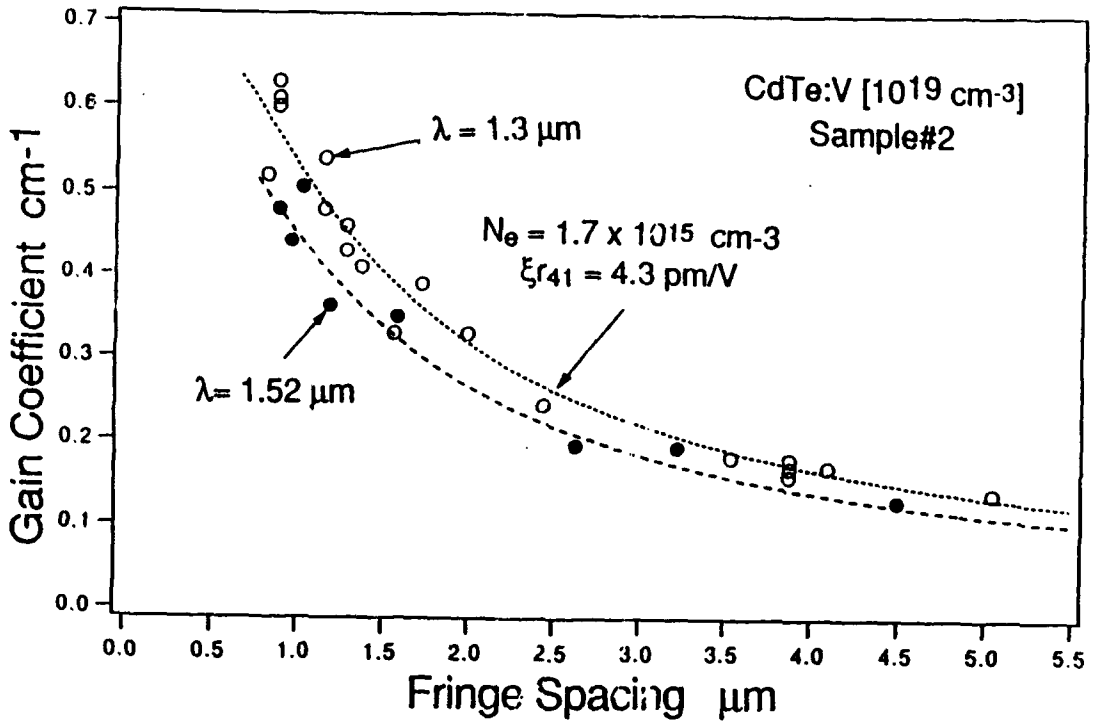

Figure 5. Measured beam coupling gain in CdTe:V at 1.3 and 1.5 μm

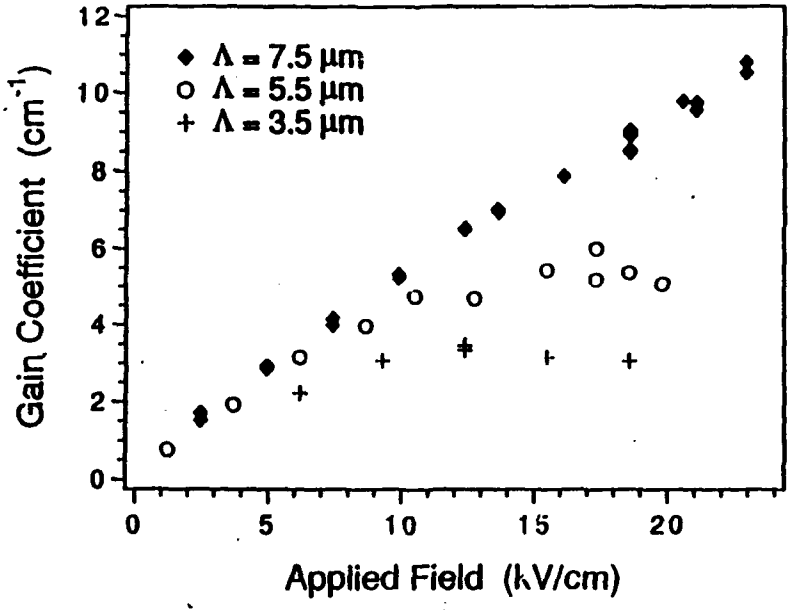

Figure 6. Alternating electric field enhanced two wave mixing gain in CdTE:V

was 10^7W-cm and the observed gain was 0.22 cm-1 at L = 1.34 mm. The absorption at 1.3 μm was less than 0.1 cm^{-1}. The derived trap density was $2x10^{15}$ cm^{-3} and xr_{41} = 3 pm/V.

The magnitude of the photorefractive index change in semiconductors is usually small and gain enhancement techniques such as dc fields or ac fields are required. We used the applied alternating field (ac) method with square and sinusoidal waveforms and report gain coefficients in excess of 10 cm^{-1} at 1.3 mm which significantly exceed the absorption coefficient of 2 cm^{-1} in our sample. This dramatic increase in the gain that can be achieved using alternating electric fields is shown in Figure 6. Our measurements show that the parameters of the ac waveform such as frequency and rise time play a significant role and can impose severe limits on the achievable gain. The limits are discussed in detail in the relevant publ

The Capacity of Photorefractive Semiconductor Interconnects.

While the semiconductors have the advantages listed above and may be the only reasonable fast, infrared, real time holographic material available, they all share the major limitation that the maximum change in the index of refraction is limited to 10^{-4} to 10^{-5}. This is in contrast to the much slower and less sensitive oxides where index changes of 10^{-2} to 10^{-3} are possible. Therefore the systems design must be such that it makes optimum use of the limited Δn and accommodates the required E fields (possibly DC or AC) required to give the maximum Δn.

We have completed a study of the possible capacity of a semiconductor interconnect based on our measurements of the photorefractive properties of the semiconductors. For limited Δn it is generally advantageous to use the assigned volume hologram approach rather than the shared volume approach. For interconnecting N inputs to N outputs, the hologram is divided into N sub-holograms each containing N gratings. Assuming the available Δn is shared equally by each grating, the strength of each grating is therefore Δn/N. The assigned volume also eliminates coherent interference effects on fan-in since the various outputs are angularly separated. To increase the Δn, one must apply either DC or alternating electric fields to the material with some sacrifice in response time.

In this analysis the number of interconnects is limited by the scattering of the material and the limited Δn. The output from any one grating must be several times the scattered intensity in that same direction. Based on this the maximum number of interconnects for the assigned volume hologram is:

$$N = 1.6\pi^3 L^3 (\Delta n)^2 / \lambda^4 \alpha_s$$

where L = interaction length

λ = the wavelength of operation

α_S = the scattering coefficient of the material.

For L = 1cm, λ = 1μm, $\Delta n = 2.4 \times 10^{-5}$, $\alpha_S = 10^{-2} cm^{-1}$, the maximum number of interconnects is

$$N_{max} = 400.$$

This can be compared to a similar calculation for the shared volume hologram which predicts a maximum capacity of 125 interconnects.

Optical Interconnections using Wave Mixing at the Bandedge in III-V Semiconductor Depletion Regions

E. Garmire

The over-arching purpose of the research we carried out under this URI contract was to seek practical means for efficient, low-power, medium-high-speed two-beam coupling that could be used in systems as an all-optical interconnect. The basis of our studies was the fact that operating at the bandedge of semiconductors gives large enhancements to the size of the nonlinearity which can be observed. Furthermore, by using internal fields within the material (such as in semiconductor depletion regions), optically induced carrier transport causes particularly sensitive nonlinearities. Therefore, our research has focused on investigating new, large and sensitive optical nonlinearities that show applicability to wave-mixing, which can then be used as all-optical interconnects.

These investigations took three directions during the URI contract, each leading to major contributions in componentry designed for use in all-optical interconnects. Our results in these three areas are summarized here.

1) Investigations of wave-mixing using photorefraction along with resonant enhancements near the band-edge in semiconductors.

Students James Millerd and Steffen Koehler demonstrated world- record photorefractive gains in iron-doped InP, using bandedge resonance enhancement along with temperature stabilization. Until this work was completed, the largest gains in III-V semiconductors, which we achieved in GaAs, required moving gratings, a difficult-to-achieve technology in which a piezo- electric motion is applied to one mirror of the two-beam coupling setup [1], or AC-switched fields, also difficult to achieve. In the work reported here [2], gains as large as 16 cm^{-1} were achieved, operating near the bandedge in InP at the wavelength of 970 nm, compatible with strained-layer lasers. The concept of our work relies on a second resonant enhancement derived from stabilizing bipolar transport in the material. This resonance was demonstrated in our studies to depend in a complex way on pump intensity, applied field, grating spacing, wavelength and temperature. The fact that such large gains were demonstrated at practical, strained-layer laser wavelengths, suggests that this technique holds considerable promise for practical optical interconnects.

We discovered, however, one drawback to using InP and similar field-dependent photorefractive nonlinearities. We found that the two-wave mixing gain is a strong junction of input beam ratio [3]. We observed a strong saturation in the nonlinear photorefractive response at high modulation depths (low beam ratios). In fact, the experimentally-measured intensity gain in a length of 4 mm of InP dropped from 1000 to 1.6 as the beam ratio dropped from 10,000,000 to 1. We found that a previously-introduced empirical formula [4] correctly modeled this behavior. The gain has the form:

$$g = g_{\infty}[1 - \exp(-am)]$$

where g_∞ is the gain measured at very high beam ratio, m is the modulation depth and a is the empirical parameter which we found here = 4.

We also investigated a phase conjugate ring resonator using this material and found that the reflectivity was limited by the combination of near bandedge losses and large signal effects to a maximum of only a few percent [5]. These results discouraged us from continuing to investigate near-band edge photorefractivity for optical interconnects, at least when used at small beam ratio or in phase conjugate resonators.

In an earlier effort, we were the first to demonstrate two- beam coupling in CdTe at the practically important wavelength of 1.5 μm [6]. We measured a gain coefficient of 2.4 cm-1 using the moving grating technique. Further work has continued by Steier's group in similar materials.

2) Nonlinearities in MQW hetero-n-i-p-i structures.

The combination of multiple quantum wells (MQW) grown as heterostructures within the depletion regions of n-i-p-i structures was shown to offer very sensitive and rather large nonlinearities [7]. For satisfactory wave-mixing suitable for optical interconnects, however, it is necessary to achieve sufficient index change that a p phase change can be accomplished. That is, the index change times the sample length must equal half a (free-space) wavelength. However, the first samples we reported saturated at an index change below what was required.

Therefore we concentrated in this URI work on investigating ways to increase the total optically-induced index change. Our approach was to combine the nonlinearity introduced by field-dependent effects (Quantum Confined Stark Effect, QCSE) with that introduced by band-filling. We achieved a combination effect that was twice as large as previously observed in hetero-n-i-p-i's. This resulted in an optically-induced absorption change of 25% per pass [8]. The data are shown in Fig. 1. For intensities below 6 W/cm^2, changes in transmission were due to the screening of built-in field in conjunction with the QCSE. For intensities greater than 30 W/cm^2, a further increase in transmission was observed due to state filling and exciton screening in the wells. There was no sign that the nonlinearity was saturating, to level of 1 kW/cm^2. The transmission changes can be related to index changes through the Kramers Kronig relations and predict that index changes of 0.05 were observed. A p phase change can be created through double- pass in 9 μm of material. Unfortunately, such long sample lengths are still not available. Furthermore, the optical powers to achieve maximum transmission changes were very large.

For these reasons we began to investigate how to make even larger nonlinearities, continuing to use QCSE modulation within n-i-p-i structures. In order to investigate the magnitude of the field-dependent effects, we decided to directly measure the near-band-edge QCSE within p-i-n structures using the same short period superlattice strained-layer InAs/GaAs MQW depletion regions we used for the n-i-p-i measurements. These studies showed results comparable to the best previously reported measurements of QCSE in strained layer MQW p-i-n structures [9,10]. From these measurements we were able to calculate that optically induced

field changes within the n-i-p-i material were much smaller than expected. Thus we embarked on a study to investigate how carriers move within p-i-n and n-i-p-i structures containing strained-layer InAs/GaAs MQW. We were particularly interested in high-speed measurements.

3) Picosecond time-resolved measurements of nonlinearities in strained-layer InGaAs/GaAs MQW p-i-n structures.

We made and reported the first picosecond time-resolved measurements of optically induced changes in QCSE in a strained InGaAs/GaAs MQW p-i-n structure as a function of applied bias [11]. Typical results are shown in Fig. 2. We found that data above 4 V could be explained by a model which assumed a rise time dominated by a single carrier sweep-out time and a decay dominated by lateral diffusion. A bias-independent electro- absorption rise time of 10 ps was obtained and appeared to be limited by the transit time of the carriers across the structure. The decay time was also 10 ps. Below 4 V the decay time increased to 80 ps as the bias was reduced to 0 V. We believe this increase may have been related to the change in depletion length with bias in the intrinsic region.

These results provide the first measurements of the ultimate response time expected for MQW-related strained layer p-i-n structures. However, several anomalous features were identified, particularly at low fields, the region of interest in n-i-p-i structures. Further research is presently underway, with JSEP funding, particulary to clarify the role of holes well as electrons in the transport in low field regimes.

The data on p-i-n measurements can be fed into a band- transport model for field screening in MQW hetero-n-i-p-i's which we introduced last year [12]. Such work is presently underway, along with further cw and pulsed measurements of MQW hetero-n-i- p-i structures. Funding for this comes from NSF.

The expected outcome of our effort, begun with URI funding and continuing with JSEP and NSF, is sufficient understanding of optically induced field screening in MQW hetero n-i-p-i materials to be able to optimize nonlinearities while maintaining high sensitivity. The results should have dramatic impact on all-optical interconnects.

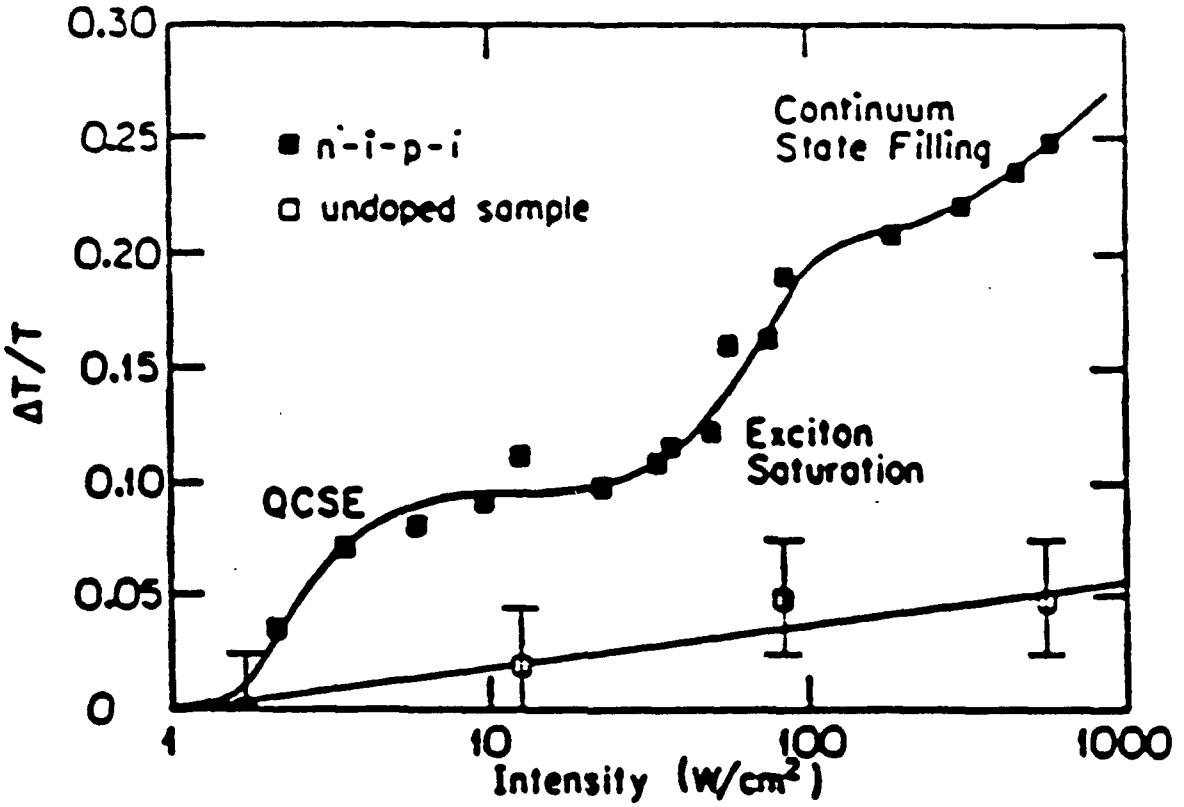

Figure 1.

Fractional transmission change in InAs/GaAs SPSLS MQW Hetero-n-i-p-i as a function of intensity, showing the first demonstration of the combined effect of several nonlinear mechanisms. At higher intensities, after the Quantum Confined Stark effect is saturated, exciton saturation causes increase in transmission. After this saturates, continuum state filling causes an increase in transmission. No saturation of this mechanism was observed. The combined effects should make possible high contrast switching with relatively low power levels.

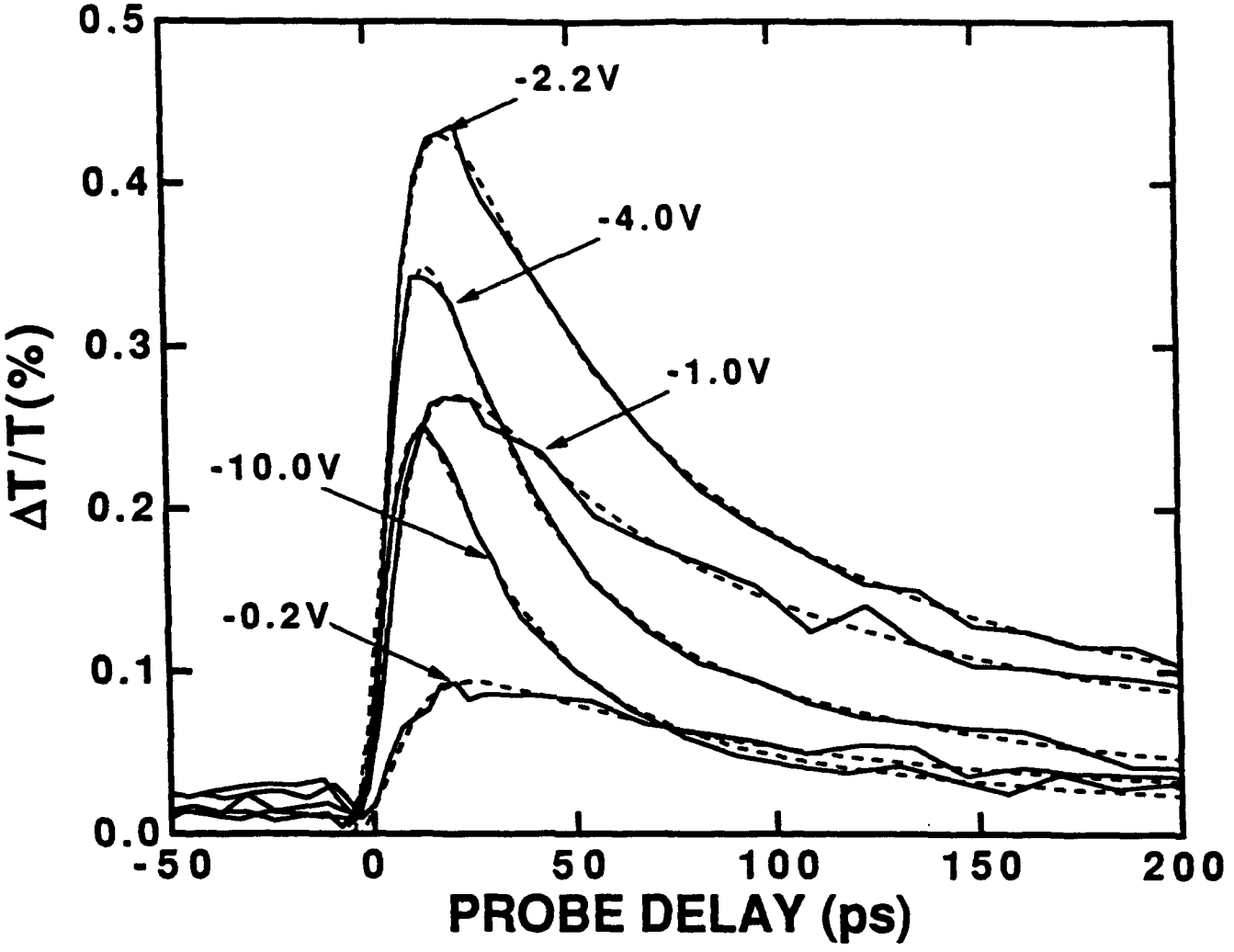

Figure 2.

Fractional transmission change in strained layer InGaAs/GaAs MQW sample as a function of probe delay time after optical excitation with 4 ps pump liberates carriers which partially screen the internal field. Fifty QW are in the i region of a p-i-n structure which was back-biased with the various voltages shown. Rise times and delay times give information on carrier transport mechanisms in diodes which contain MQW.

Photorefractive Optical Interconnections

J. Feinberg

Programmable optical interconnections using phase conjugation:

We constructed a device to connect any of N input channels to any of M output channels. The device uses a photorefractive crystal of $BaTiO_3$ as a mutually-pumped phase conjugator in a "bird-wing" geometry. One simply directs light into each pair of channels and the conjugator automatically connects them. The two injected light beams should have the same nominal wavelength but need not be coherent with each other.

We used a tapered fiber to combine and scramble all of the incoming signals before they reach the phase conjugator. Scrambling makes the spatial overlap of all of the channels uniform, so that the throughput of the device is the same for any channel. We use the unscrambling capability of the phase conjugator to direct the signal to the proper output channel. The overall system transmissivities, including losses from coupling into and out of each of the 8 different input fibers, were a few percent, and were smaller than the transmissivities of the conjugator alone by a factor of 5. The reduced transmissivity was due to the fact that the beam headed from the crystal into a fiber taper was an imperfect phase-conjugate replica of the beam coming out of the taper, caused partly by the imperfect collection of each fiber's light by our small-aperture objectives, but especially by the easily observable scattering at the cleaved end of the fiber tapers. The resulting loss of information caused imperfect phase-conjugate reconstruction, which then caused inaccurate coupling back into the tapered fiber. To improve the overall transmissivities, we need well-cleaved or even polished fiber tapers and objective lenses having a large numerical aperture. A more problematical result of the imperfect fiber cleave was that it produced interchannel crosstalk. Light lost from scattering at the cleave prevented the phase conjugator from aiming all of the light to the correct channel. The typical measured interchannel crosstalk was ~ 15% (defined here as the signal power in an incorrect channel divided by the signal power in the correct channel). Again, by collecting a larger fraction of the light coming from the taper fiber and by reducing the scattered light, the interchannel crosstalk can be reduced to tolerable levels.

The transmission bandwidth of this device is limited by the modal dispersion of the fiber taper, the Bragg-matching bandwidth of the photorefractive grating in the crystal, and the group velocity dispersion of the crystal. When using rapidly modulated light to establish the grating, the modal dispersion of the fiber taper will decrease the spatial coherence of the light coming out of the fiber taper, and this will decrease the interconnection efficiency. We estimate that a one-meter long multimode fiber taper having a numerical aperture of 0.22 limits the maximum data rate to 200 Gb/sec. For a sufficiently short fiber taper the data rate is then limited by the finite Bragg-matching bandwidth of the photorefractive grating, which we estimate to be 1 THz, corresponding to a maximum data rate of 1000 Gb/sec. Using the known group-velocity dispersion in $BaTiO_3$ of 7.266 (ps^2/m) for e rays at 515 nm, we calculate that for a 5 mm long crystal the maximum data rate is 3000 Gb/sec.

Experimentally we successfully operated the bird-wing conjugator without the fiber taper using sub-picosecond pulses from a sync-pumped dye laser, which corresponds to a data rate of ~1000 Gb/sec. We also calculate that the coupling efficiency of the signal back into the tapered fiber will decrease and interchannel crosstalk will markedly increase if the wavelength difference of the A and B channel lasers exceeds 0.5 nm.

In summary, we have demonstrated a fiberoptic interconnection device based on mutually-pumped phase conjugator. The conjugator automatically routes light from selected information-sending channels to selected information-receiving channels, and vice versa. The phase-conjugating property of the device eliminates the need for critical alignment. In principle, we can make the device very compact, and so interconnect a large number of optical fiber channels.

Time-Resolved Holography:

We demonstrated a holographic "light shutter" that selectively displays objects according to their arrival time. One could use such a shutter with a pulsed light source to reveal an object embedded in a dense scattering medium (such as an airplane concealed in fog or a tumor buried in tissue).

The device exploits spectral hole-burning in an inhomogeneously broadened absorber. We used the organic dye protoporphyrin doped into a solid block of polystyrene. Each dye molecule acts as a lightly-damped resonator, but due to inhomogeneities in the plastic matrix, each dye molecule has a slightly different resonant frequency. If cooled to a temperature of 2° K, the phase-relaxation time of the molecule's upper level becomes quite long ($T_2 \approx 1$ nanosecond), so that each absorption has a narrow homogeneous spectral width of $\Delta\omega = 1/(\pi T_2) \cong 0.01 cm^{-1}$. The polystyrene matrix causes the net absorption spectrum of all of the molecules to form an inhomogeneously broadened band extending over a 200 cm^{-1} wide range. This material resembles a bank of 20,000 narrow-band resonators, and we use this spectral hole-burning material to record and store the spectral and spatial contents of an incident light beam.

In our experiments we used a 3-mm thick block of polystyrene doped with protoporphyrin at a concentration of 10^{-3} moles/liter. The light source was a continuous-wave modelocked Nd:YAG laser which synchronously pumped a tunable dye laser to produce pulses having an intensity temporal width of 8 picoseconds (FWHM). (These pulses were not transform limited; they had a coherence width of only 0.5 picoseconds). The repetition rate of the laser pulses was 76 Mhz. A beamsplitter divided the beam from the picosecond dye laser into a reference beam and a separate beam to illuminate the various objects in the scene.

The recorded scene consisted of two objects, as shown in Fig. 1. The nearby object was a 1.0-mm thick glass slide with the letters "HOLO" attached to its front surface. The distant object was a white paper screen carrying the letters "GRAM", which was pressed against the back of the transparent slide, so the separation between the two objects was about 1 mm. In order to increase the amount of light scattered by the slide, its front surface was coated with a Christmas frosting aerosol

spray. The slide was illuminated from the front. Of the scattered light from the slide reaching the polystyrene block, about 80% came from the front sprayed surface of the slide, and only 20% came from the rear surface. However, the scattered light from the front of the slide reached the storage medium 10 picoseconds (twice the glass travel-through time) before light from the back of the slide. We used this time delay to block out the early-arriving light. In the first experiment a hologram was recorded with the reference beam timed to arrive before both of these object waves. Viewing the laser-illuminated slide by eye from the position of the polystyrene block, one could clearly read the words "HOLO", but the intense glare from the front surface almost completely obscured the letters "GRAM" located near the back of the slide. (This is in analogy with the glare caused by the bookseller's glass window obscuring the titles of the books located behind the window.) In the second experiment a hologram was recorded with the reference beam carefully timed to arrive within the 10 picosecond interval between the two object waves. Now only the distant object is reconstructed, and the nearby object was eliminated.

We emphasize that the light from these objects need not arrive at the polystyrene block at the same time as light in the reference pulse in order to for the hologram to be recorded. In fact, because the coherence time of the light pulses was only 0.5 ps, and because we set the reference beam to arrive at the storage medium about 5 ps before the light from the back of the slide, the reference and object beams did not produce a conventional intensity interference pattern in the storage medium. We note that the maximum time delay permitted between the object and reference beams was 10^3 ps and is set by the phase-decay time T_2 of the sample.

In our experiments we selectively reconstructed those objects that sent light to the hologram *after* the reference pulse had arrived. However, for some applications it is desirable to do the opposite and recreate the light that arrived *before* the reference pulse. For example, consider the problem of imaging an object that is embedded in a scattering medium, such as a tumor embedded in breast tissue. Illuminate the tissue from behind with a short laser pulse. Light transmitted through the tissue without any scattering will emerge before light that has been multiply scattered by the tissue. Because the eye records all of this light, and because the scattered light overwhelms the unscattered light, the tumor remains unseen. However, if light that arrived earlier at the eye could be selectively enhanced, than a shadowgram of the tumor would become visible.

We can preferentially select early light over late light by simply altering the direction of the read-out beam used in the experiments above. Instead of using a read-out beam that is in the same direction as the reference beam, one should use a read-out beam that is directed exactly opposite to the direction of the original reference beam. This is the "four-wave mixing" geometry of traditional phase-conjugation experiments, but with a spectral hole-burning material now only those portions of the object that arrived *before* the reference beam will be holographically reconstructed in the final image. In this way light scattered from back-lighted tissue could be eliminated, while light traveling directly through the tissue could be preserved, and would form a shadowgram of features embedded in the tissue. We caution that this scheme requires a very large dynamic range for the hologram, because in thick tissue the scattered light can be much more intense than the unscattered light. We estimate

that our present spectral hole-burning medium has a limited dynamic range of about 10^3.

High-brightness output from a laser diode array using optical phase conjugation:

Although laser diode arrays can produce impressive amounts of optical power, they usually operate simultaneously on many transverse modes, which makes their far-field pattern a mess. Their poor beam quality makes laser diode arrays ill suited for many applications, such as launching intense light into single-mode waveguides or pumping mini-laser systems.

We coupled a laser diode array to an external, photorefractive phase conjugator, and thereby forced the array to operate on a single transverse mode. Even while running close to its maximum rated output power, this device put out a near diffraction-limited beam.

We used a 1 Watt, 20-stripe, laser diode array (Spectra Diode Labs 2461-P1 with no special coatings) mounted on a heat sink. The array of lasers formed a line in the horizontal plane, and the laser's output is polarized along this line. We used additional optics to make the polarization and the coherence axes of the light both lie in the plane defined by the $BaTiO_3$ crystal's c-axis and the direction of the incident beam. The crystal acted as a self-pumped phase conjugator and returned light exactly back into the gain region of the laser diode array.

When we first switched on the laser, its output was that of a usual, free-running laser diode array: Fig. 2(a) shows its poorly defined, twin-lobed, far-field pattern (~40 times the diffraction limit of the 200 μm emitting region). After a short delay (typically 20 seconds), the phase conjugator turned on, and one of the far-field lobes grew at the expense of the other. After an additional ~50 seconds the phase conjugate reflectivity attained its steady-state level, and the laser settled into single-lobed operation, as shown in Fig. 2(b).

Once the phase-conjugate mirror turned on, it tracked in real time small changes in the laser's far field profile or in the aperture's position. The array maintained single-lobe emission for all driving currents. Our maximum driving current was 1.5 A (3.1 I_{th}), which produced a total array output power of 910 mW. (We limited the driving current to 1.5A to avoid the possibility of intensity damage to the array facet.) At these high output powers the far-field lobe width gradually increased up to 1.5 times the diffraction limit and contained 54% of the array's output power.

The external cavity output exhibited surprising intensity stability (<0.5% fluctuations) over a time scale ranging from a few seconds to hours. The dynamic response of the phase-conjugate mirror compensated for gradual changes in the drive current, operating wavelength, or ambient temperature with no degradation in the single lobe profile. The phase conjugator ensured that all of the light fed back to the laser was coupled into natural modes of the laser. In close analogy to conventional injection locking of a laser diode array, the asymmetry of the feedback in this external cavity caused a preferential direction of emission at the same angle as the aperture window, but on the opposite side of the normal to the array facet.

In summary, we developed a technique for obtaining stable, near diffraction-limited output from a high-power laser diode array. Because the laser emits only a small fraction of its output into the conjugator itself, we envision that the output power can be significantly increased without damaging the conjugator. The ability of the phase conjugator to feed light back to precisely the high-gain region of the laser should allow the extension of this technique to much larger arrays, or to more complicated, higher-power diode-laser structures, and this is the current direction of our investigations.

CV

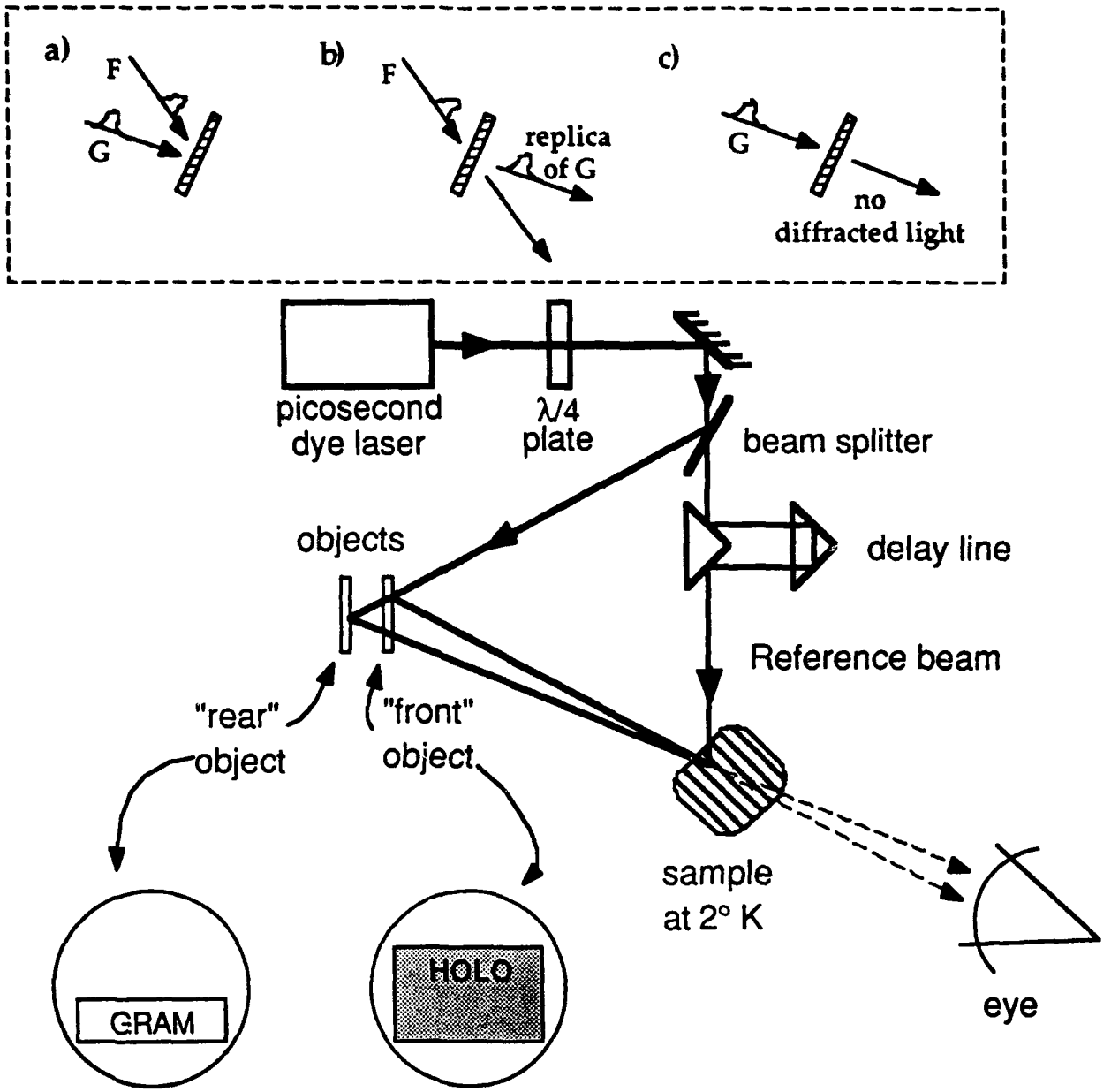

Figure 1) Seeing a distant object through a scattering medium using temporal holography. The inset shows the timing of the object (G) and reference (F) pulses. Only light that arrives at the sample *after* the reference pulse will be later reconstructed upon readout.

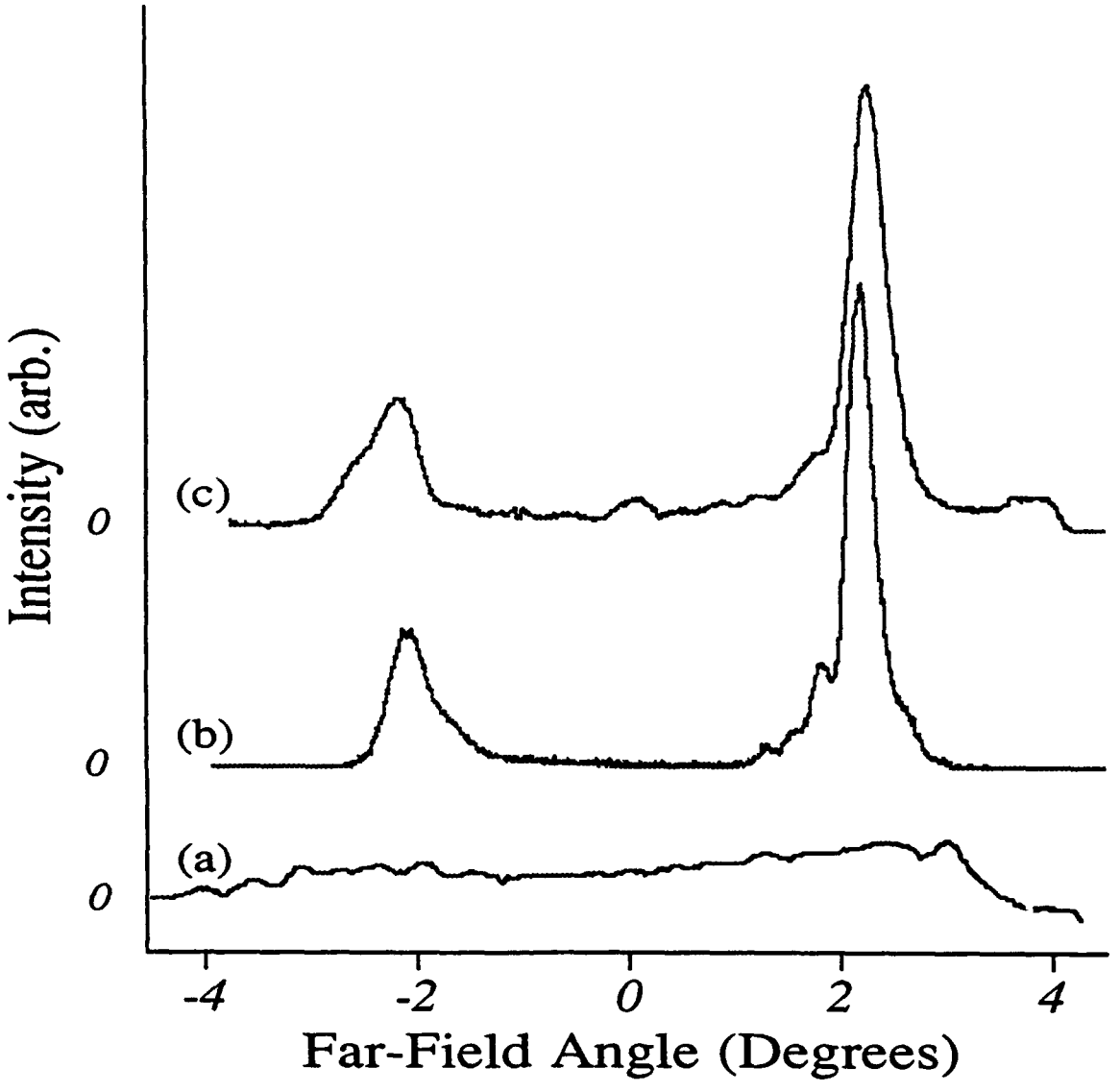

Figure 2) Far-field output patttern of a laser diode array (a) with no phase-conjugate feedback (note the wide angular spread of the emitted light), (b) with phase conjugate feedback (note the narrow output beam), and (c) at higher current with phase-conjugate feedback. The traces have been displaced vertically for clarity. The large spike in (b) and (c) is the almost-diffraction-limited output beam. The smaller bump is the light directed to the phase conjugating crystal.

Transmission of many Wavelength-Division-Mutiplexed Channels through a Cascade of Erbium-Doped Fiber Amplifiers in an Optical Switching System

A. Willner

Erbium-doped fiber amplifiers (EDFA's) have revolutionized both long-distance and distribution-based optical communication systems. Furthermore, optically-amplified systems can have a dramatic increase in the total capacity by incorporating wavelength-division-multiplexing (WDM). However, transmitting many WDM amplified channels is difficult to implement since the EDFA gain is wavelength dependent whereas the link loss (due to optical splitting, component insertion loss, and fiber attenuation in a distribution network) is wavelength independent. Such a gain/loss wavelength discrepancy will result in a severe SNR differential among many WDM channels after propagating through a cascade of EDFA's. A large SNR differential is undesirable since (a) an equalized system will result in a high SNR for many more WDM channels than will an unequalized one, and (b) a limited system power margin or receiver dynamic range may cause system impairments.

Optical computing and switching systems can benefit by the implementation of WDM and EDFA's in much the same way that distribution networks can: WDM increases data transfer capacity and EDFA's compensate for any splitting, insertion, and fiber losses. We will discuss two projects related to the problem of implementing WDM and EDFA's in an optical computing system due to the EDFA's non-uniform gain.

1) Passive equalization of non-uniform EDFA gain by optical filtering for transmission of 20 WDM channels through a cascade of EDFA's

We have analyzed the performance of several transmission and notch optical filters for equalizing the non-uniform EDFA gain in a WDM cascaded-amplifier system. For 20 WDM channels spaced 0.5 nm apart, it is found that 3-dB, 2-nm-wide notch filters with center wavelengths at 1.560 μm will provide equalized SNR performance for potential multi-user distribution when located after every group of 20 EDFA's. This filter center wavelength is chosen because it is the location of a newly-generated spectral peak in an amplifier cascade. We find that 19 channels can be equivalently transmitted through 100 EDFA's, and 7 channels can be transmitted over 200 EDFA's with a range in SNR's of 6 and 4 dB, respectively. *A priori* knowledge of the exact nature of the input or output signals is not required.

The amplified spontaneous emission (ASE) power levels of a single EDFA are non-uniform over much of the spectrum including a peak at 1.531 μm and a relatively-flat "shoulder" centered at ~1.558 μm. After 100 amplifiers, two general peaks are present, one at 1.531 μm (which has narrowed), and a second near 1.560 μm. After propagating through 200 amplifiers, however, the 1.531-μm peak becomes severely attenuated and the 1.560-μm peak dominates.

Based on the peaks which appear in the ASE, an inverse-Lorentzian-shaped notch filter can be placed after each amplifier and centered at 1.531 μm to attenuate

the ASE peak existing after a single amplifier, or it can be placed at 1.560 μm to attenuate the new peak which arises after propagating through a cascade of amplifiers; note that transmission filters do not generally improve performance. Since the gain peak at 1.531 μm becomes attenuated regardless in an unfiltered amplifier cascade, the notch filter at 1.531 μm does not significantly improve performance.

Figures 1a shows the SNR after 100 amplifiers as a function of wavelength given notch filters located at 1.560 μm. The notch filter located at 1.560 μm provides good SNR equalization. By placing a simple 0.15-dB notch filter after each amplifier, we can significantly equalize the SNR for the different channels in which all 20 channels fall within an 8-dB range; this is in comparison to 16-dB SNR range for the unfiltered case. Since it is difficult to fabricate a notch filter of such a shallow (0.15-dB) depth, we find that even if a 3-dB notch filter is placed after every group of 20 EDFA's and providing the same attenuation at 1.560 μm, the SNR's are still similarly equalized. Equalization can also be accomplished for transmitting 7 WDM channels through 200 amplifiers, a significant improvement over a non-filtered system. Figure 1b compares the SNR of the 7 most-equalized channels for the 1.560-μm notch filter case with the unfiltered case. The range of SNR's for these channels is <4 dB and >23 dB for, respectively, the notched and unfiltered cases, demonstrating a substantial improvement by using the notch filter.

2) Guidelines for optimizing system performance for 20 WDM channels propagating through a cascade of EDFA's

In general, it remains ambiguous as to what optimal values should be chosen for the many system variables in an optically-amplified WDM system to maintain a high SNR as well as a low degree of SNR differential between channels; although techniques exist for SNR equalization, we seek to optimize the system variables without resorting to external methods.

We have analyzed 20 WDM channels passing through a cascade of 100 EDFA's and find the optimal conditions for achieving a high SNR for as many channels as possible. Since many of these parameters are inter-dependent, we attempt to isolate the effects each one has on the system performance. We find that the link loss is the most critical parameter for narrowing the SNR differential between the 20 channels (i.e. most equalized SNR performance). Furthermore, values near 20-dB unsaturated small-signal gain for each amplifier provide the highest overall SNR for the 20 channels. Additionally, pump wavelengths of 0.98 or 1.48 μm can be equivalently used, and the cascade performs well with moderate pump and signal powers.

When considering slight changes in a given variable, the system performance is most sensitive to the link loss between amplifiers; this link loss represents component insertion losses plus either the fiber attenuation or a distribution split. In a single-channel system, the link loss significantly affects the relative peaks occurring in the ASE and gain spectra; note that the 1.531-μm gain peak of a typical EDFA does not become attenuated if the link loss is too high whereas the newly-generated 1.5625-μm peak appearing in an EDFA cascade will overwhelmingly dominate if the link loss is too low. Since different EDFA-gain wavelengths will peak for different link losses, a

"see-saw" effect will occur for our 20-channel system, with the SNR's becoming skewed in one direction or another given either a high or low link loss. Figure 2a shows the SNR's for the 20 WDM channels after 100 amplifiers for different link losses. Two peaks are present, one near 1.554 μm and a stronger one near 1.560 μm; these dual peaks are an artifact of the different wavelength dependencies in the absorption and emission cross-sections of Erbium. Figure 2b shows the SNR as a function of link loss for the five defining extreme channels (namely the two peak points at 1.554 and 1.560 μm and the three valley points at 1.553, 1.557, and 1.5625 μm), with the value at which the five lines form the smallest SNR differential being the optimal link loss. These figures illustrate that the SNR's are quite sensitive to the link loss, and that the optimal link loss for high as well as equalized SNR's across all the channels is 10.5 dB for a 20-dB small-signal gain.

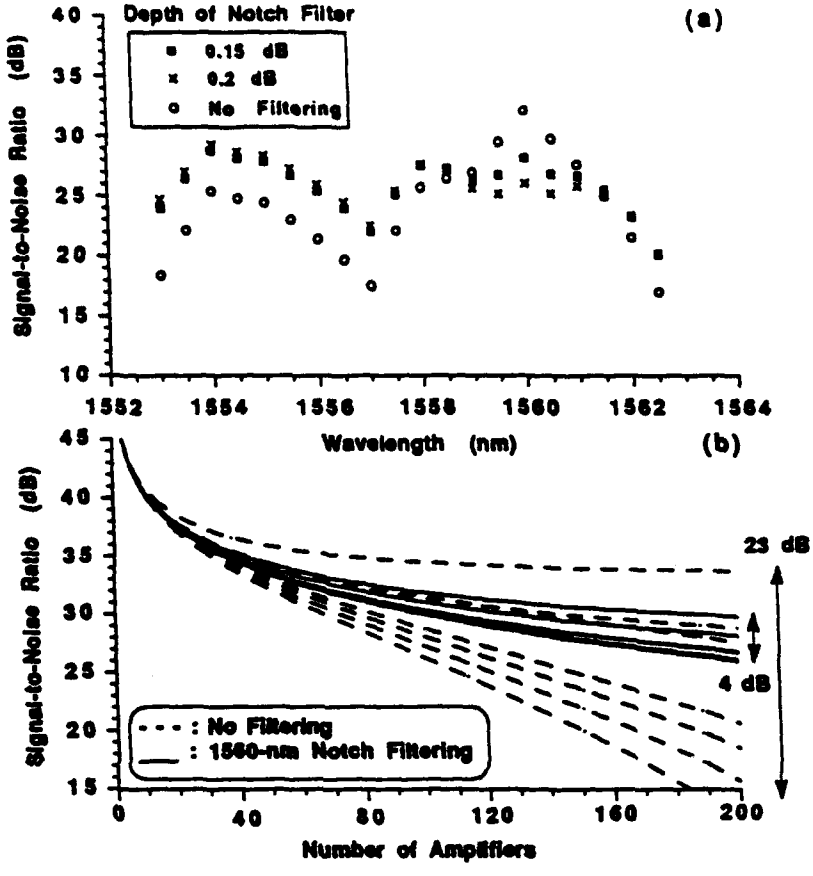

Figure 1.

(a) SNR for the 20 WDM channels for which in-line notch filters are located at 1.560 μm. The passband is 2 nm.

(b) SNR versus number of amplifiers in the cascade for the 7 most equalized channels in the cases with 1.560-μm notch filters and without any filters.

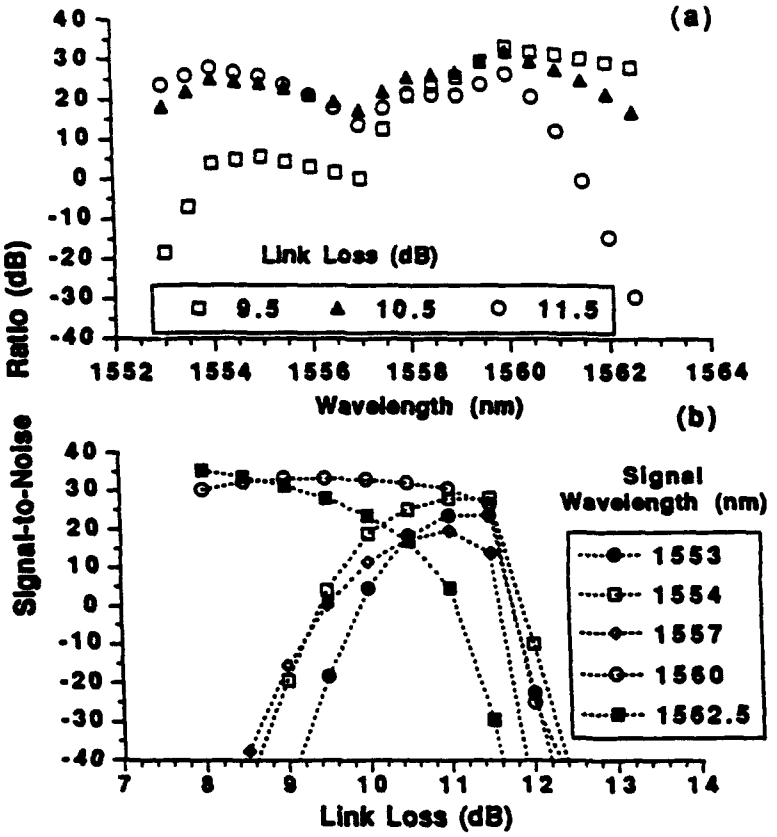

Figure 2.

(a) SNR for the 20 WDM channels after passing through 100 amplifiers for inter-amplifier link losses of 9.5, 10.5, and 11.5 dB.

(b) SNR versus link loss for the five defining channels.

CENTER FOR THE INTEGRATION OF OPTICAL COMPUTING

PUBLICATIONS

1. S.-M. Hwang and A. E. Willner, "Guidelines for Optimizing System Performance for 20 WDM Channels Propagating through a Cascade of EDFA's," *IEEE Photonics Technology Lett.*, vol. 5, no. 10, Oct., 1993.

2. S.-M. Hwang and A. E. Willner, "Guidelines for Optimizing System Performance for 20 WDM Channels Propagating through a Cascade of EDFA's," Conference of the IEEE Lasers and Electro-Optics Society, Nov. 1993, San Jose, CA (IEEE, Piscataway, New Jersey, 1993).

3. A. E. Willner and S.-M. Hwang, "Passive Equalization of Non-Uniform EDFA Gain by Optical Filtering for Megameter Transmission of 20 WDM Channels through a Cascade of EDFA's," *IEEE Photonics Technology Lett.*, vol. 5, no. 8, Sept., 1993.

4. A. E. Willner and S.-M. Hwang, "SNR Equalization of 20 WDM Channels Propagating Through a Cascade of EDFA's," Meeting of the Optical Society of America, *Tech. Dig.*, Toronto, Canada, Oct. 1993 (Optical Society of America, Wash., D.C., 1993).

5. A. E. Willner and S.-M. Hwang, "Passive Equalization of Non-Uniform EDFA Gain by Optical Filtering for Megameter Transmission of 20 WDM Channels through a Cascade of EDFA's," Conference on Optical Amplifiers and Their Applications, Proceedings, Yokohama, Japan, July, 1993 (Optical Society of America, Wash., D.C., 1993).

6. A. E. Willner, "Approaches to Switching and Amplification in WDM Systems," Invited Paper, IEEE Lasers and Electro-Optics Society Annual Meeting, *Technical Digest*, pp. 82-84, Boston, MA, Nov. 1992 (IEEE/LEOS, Piscataway, New Jersey, 1992).

7. A. E. Willner, "WDM Amplification and Switching," Invited Paper, Society of Photo-Instrumentation Engineers (SPIE) Conference on Multigigabit Fiber Communications, *Technical Digest,* paper 1787-01, pp. 2-19, Sept., 1992, Boston, MA (SPIE, Bellingham, Wash., 1992).

8. A. Partovi, A. Kost, E. Garmire, G. Valley, and M. Klein, *Appl. Phys. Lett.* 56, 1087 (1990).

9. James E. Millerd, Steffen D. Koehler, Elsa Garmire, Afshin Partovi, Alastair M. Glass and Marvin B. Klein, "Photorefractive gain enhancement in InP:Fe using band-edge resonance and temperature stabilization", *Appl. Phys. Lett.* 57 (26) (1990).

10. James E. Millerd, Elsa Garmire, and Marvin Klein, "Investigation of photorefractive self-pumped phase-conjugate mirrors in the presence of loss and high modulation depth", *J. Opt. Soc.* Am. B, Vol. 9, No.8 (1992).

11. Ph. Refregier, L. Solymar, H. Rajbenback and J.P. Huignard, "Two beam coupling in photorefractive $Bi_{12}SiO_{20}$ crystals with moving grating: theory and experiment", *J. Appl. Phys.* 58, 45 (1985).

12. James E. Millerd, Elsa M. Garmire, and Marvin Klein, "Self-pumped phase conjugation in InP-Fe using band-edge resonance and temperature stabilization: theory and experiments", *Opt. Lett.* Vol. 17, 100 (1992).

13. Afshin Partovi, James Millerd, Elsa Garmire, Mehrdad Ziari, William Steier, Sudhir Trivedi, and Marvin Klein, "Photorefractivity at 1.5μm .n CdTe:V", *Appl. Phys. Lett.* 57 (9) (1990).

14. A. Kost, E. Garmire, A. Danner, and P.D. Dapkus, *Appl. Phys. Lett.* 52, 637 (1988).

15. Alan Kost, Michael Jupina, Elsa Garmire, T.C. Hasenberg, "Combined local and carrier transport optical nonlinearities in hetero n-i-p-i structure", Appl. *Phys. Lett.* 58 (10), (1990).

16. Michael Jupina, Elsa Garmire, Tom C. Hasenberg, and Alan Kost, "InAs/GaAs short-period strained-layer superlattices grown on GaAs as quantum confined Stark effect modulators", *Appl. Phys. Lett.* 60 (6), (1992).

17. S. D. Koehler, E.M. Garmire, M.H. Jupina, T.C. Hasenberg, and A.R. Kost, "Direct Interferometric measurements of quantum-confined stark effect in InAs/GaAs short period strained-layer superlattice MQWs", *Elect. Lett.* Vol. 27, 2302 (1991).

18. Daniel Mahgerefteh, Ching-Mei Yang, Li Chen, Kezhong, Wei Chen, E. Garmire and A. Madhukar, "Picosecond time-resolved measurements of electroabsorption in an InGaAs/GaAs multiple quantum well p-i-n modulator", *Appl. Phys. Lett.* 61 (21), (1992).

19. Daniel Mahgerefteh and Elsa Garmire, "Band-transport model for field screening in multiple-quantum-well hetero-n-i-p-i's", *Opt. Lett.* Vol. 18, 616, (1992).

20. A. Rebane and Jack Feinberg, "Time Resolved Holography," *Nature* 351, 378-380 (1991).

22. S. MacCormack and J. Feinberg, "High-Brightness Output From A Laser-Diode Array Coupled To A Phase-Conjugating Mirror," *Opt. Lett* 18, 211-213 (1993).

23. Li Chen, Kezhong Hu, R. M. Kapre and A. Madhukar, "High contrast ratio self electro-optic effect devices based on inverted InGaAs/GaAs asymmetric Fabry-Perot Modulators", *Appl. Phys. Lett.* 60, 422 (1992).

24. L. Chen, K.Z. Hu, R.M. Kapre, W. Chen, and A. Madhukar, "High Contrast Optically Bistable Optoelectronic Switches Based on InGaAs/GaAs(100) Conventional

and Inverted Asymmetric Fabry-Perot Modulators Grown via Molecular Beam Epitaxy", *Jour. Vac. Sc. Tech.* B 10, 1014 (1992).

25. K.Z. Hu, L. Chen, K. Kaviani, P. Chen, and A. Madhukar, "All Optical Photonic Switches Using Integrated Inverted Asymmetric Fabry-Perot Modulators and Heterojunction Phototransistors", *IEEE Photonics Technology Letters*, Vol 4, 263 ,1992.

26. Kezhong Hu, Li Chen, K. Kaviani, P. Chen, A. Madhukar, "All-optical photonic switches by the monolithic integration of inverted asymmetric Fabry-Perot modulators/detectors and heterojunction phototransistors" *CLEO Technical Digest Series*, (Optical Society of America, Washington, DC, 1992), Vol.12, p.18.

27. R.M. Kapre, L. Chen, K. Kaviani, K.Z. Hu, P. Chen, and A. Madhukar, "High Contrast Optically Bistable Optoelectronic Switches Using Strained InGaAs/AlGaAs Materials System", MRS Symp. Proc. 240, 875 (1992).

28. K. Hu, Li Chen, K. Kaviani, Q. Xie, K. C. Rajkumar, W. Chen, R. F. Cartland, P. Chen, and A. Madhukar, "Electroabsoption behavior of strained InGaAs/AlGaAs multiple quantum wells and their application as resonant cavity in Fabry-Perot light modulators" Proceedings of the 21th International Conference on the Physics of Semiconductors, Eds. P. Jiang and H. -Z. Zheng (World Scientific Publishing Co. PTE LTD., Singapore, 1992), p.1270.

29. D. H. Rich, K.C. Rajkumar, Li Chen, A. Madhukar and F.J. Grunthaner, "Defects in strained In0.2Ga0.8As/GaAs multiple quantum wells on patterned and unpatterned substrates: A near-infrared cathodoluminescence study," *J. Vac. Sci. Technol.* 10, 1965 (1992).

30. D. H. Rich, K.C. Rajkumar, Li Chen, A. Madhukar and F.J. Grunthaner, "Near-infrared cathodoluminescence imaging of defect distributions in In0.2Ga0.8As/GaAs multiple quantum wells grown on prepatterned GaAs," *Appl. Phys. Lett.* 61, 222 (1992)

31. K. Hu, R. Cartland, Li Chen, K. Kaviani, P. Chen, and A. Madhukar, "Ex-situ cavity phase tuning of InGaAs/AlGaAs multiple quantum well based inverted asymmetric Fabry-Perot reflection modulators, "Presented at the IEEE/LEOS & OSA topical meeting of Spatial Light Modulators and Applications, March 15-17, 1993, Palm Springs, California.

32. K. Kaviani, L. Chen, K. Hu, Q. Xie, and A. Madhukar, " Effect of structural and chemical parameters on the optical properties of highly strained AlGaAs/InGaAs/AlGaAs quantum wells", *J. Vac. Sci. Technol.* B 11(3), 805(1993).

33. L. Cheng and A.A. Sawchuk, "Three-Dimensional Omega Networks for Optical Implementation," Applied Optics, vol. 31, pp. 5468-5479, (1992).

34. L. Cheng and A.A. Sawchuk, "A One-Copy Algorithm for 2-D Shuffles for Optical Omega Networks," *Journal of Parallel and Distributed Computing*, vol. 16, pp. 54-66, (1992).

35. M. Govindarajan, S.R. Forrest, L. Cheng and A.A. Sawchuk, "Optically Powered 2x2 Optoelectronic Switch with Polarization Routing," *IEEE Photonics Technology Letters*, vol. 3, pp. 669-672, (1991).

36. J.-M. Wang, L. Cheng and A.A. Sawchuk, "Optical Two-Dimensional Perfect Shuffles Based on a One-Copy Algorithm," *Applied Optics*, vol. 31, pp. 5464-5467, (1992).

37. J.-M. Wang, L. Cheng, and A.A. Sawchuk, "Light Efficient Two-Dimensional Perfect Shuffles with DuPont Photopolymer Holograms," to appear in *Applied Optics*.

38. A.S. Miller, L. Cheng and A.A. Sawchuk, "Space Multiplexing in Multistage Optical Networks," *Technical Digest, ICO Topical Meeting on Optical Computing*, Minsk, Belarus, June 29 - July 1, 1992.

39. M. Govindarajan and S. R. Forrest, "Optically Powered Arrays for Optoelectronic Interconnection Networks", *Applied Optics*, vol. 30, 1335 (1991).

40. J. J. Brown, J. Gardner and S. R. Forrest, "Optically Powered, Integrated "Smart" Pixels for Optical Interconnection Networks", *IEEE Photonics Technol. Lett.*, vol. 3, 1136 (1991).

41. J. J. Brown, J. Gardner and S. R. Forrest, Topical Mtg. on Int. Photonic Res. *Tech. Dig.*, vol. 8, 11 (1991).

42. K. M. Dzurko, E. P. Menu, C. A. Beyler, J. S. Osinski, and P. D. Dapkus, " "Low threshold quantum well lasers grown by metalorganic chemical vapor deposition on nonplanar substrates," (1989).*IEEE J. Quantum Electron.* **25**, 1450 (1989).

43. N. C. Frateschi, J. S. Osinski, C. A. Beyler, P. D. Dapkus, "Low-threshold single-quantum-well InGaAs/GaAs lasers grown by metal-organic chemical vapor deposition on structured substrates," *IEEE Photon. Technol. Lett.* **4**, 209 (1992).

44. N. F. Frateschi, S. G. Hummel, P. D. Dapkus, "In-Situ Laser Reflectometry Applied to the Growth of $Al_xGa_{1-x}As$ Bragg Reflectors by Metalorganic Chemical Vapor Deposition,"*Elec. Lett.* **27**, 155 (1991).

45. N. C. Frateschi and P. D. Dapkus, S. S. Ou, J. J. Yang, and M. Jansen, "Low threshold InGaAs/GaAs 45° folded cavity surface emitting laser grown on structured substrates,"*IEEE Photonics Tech. Letters* **5**, 738 (1992).

46. N. C. Frateschi and P. D. Dapkus, S. S. Ou, J. J. Yang, and M. Jansen, "Analysis of non-planar wave propagation through multilayer Bragg reflectors for folded cavity and vertical cavity surface emitting laser structures,"*IEEE J. Quantum Electron.*, in press.

47. C. H. Wang and B. K. Jenkins, "Subtracting Incoherent Optical Neuron Model: Analysis, Experiment, and Applications," *Applied Optics,* Vol. 29, No. 14, pp. 2171-2186 (10 May 1990).

48. D. J. Wiley, I. Glaser, B. K. Jenkins, A. A. Sawchuk, and A. Weber, "Lenslet array based dynamic optical neural network," Conference Digest, 1990 International Topical Meeting on Optical Computing, International Commission for Optics, SPIE Vol. 1359, pp. 245-246 (1990).

49. B. K. Jenkins, G. C. Petrisor, S. Piazzolla, P. Asthana, and A. R. Tanguay, Jr., "Photonic Architecture for Neural Nets Using Incoherent/Coherent Holographic Interconnections," Conference Digest, 1990 International Topical Meeting on Optical Computing, International Commission for Optics, SPIE Vol. 1359, pp. 317-318 (1990).

50. P. Asthana, H. Chin, G. Nordin, A. R. Tanguay, Jr., S. Piazzolla, B. K. Jenkins, and A. Madhukar, "Photonic Components for Neural Net Implementations Using Incoherent/Coherent Holographic Interconnections," Conference Digest, 1990 International Topical Meeting on Optical Computing, International Commission for Optics, SPIE Vol. 1359, pp. 323-324 (1990).

51. B. K. Jenkins and A. R. Tanguay, Jr., "Photonic Neural Networks with Incoherent/Coherent Holographic Interconnections," Korea-USA Joint Workshop on Optical Neural Networks, Seoul, Korea, April 15-19, 1990.

52. D. J. Wiley, I. Glaser, B. K. Jenkins, and A. A. Sawchuk, "Incoherent Dynamic Lenslet Array Processor for Neural Networks," Annual Meeting of the *Optical Society of America, paper* FDD1, San Jose, Calif., Nov. 4-9, 1991.

53. S. Piazzolla, B. K. Jenkins, and A. R. Tanguay, Jr., "Single-Step Copying Technique for Multiplexed Volume Holograms," Annual Meeting of the *Optical Society of America, paper* TuH2, San Jose, Calif., Nov. 4-9, 1991.

54. B. K. Jenkins and A. R. Tanguay, Jr., "Photonic implementations of neural networks," in Neural Networks, for Signal Processing, B. Kosko, editor (Prentice-Hall, Englewood Cliffs, NJ, 1992) Chap. 9, pp. 287-382.

55. D. J. Wiley, I. Glaser, B. K. Jenkins, and A. A. Sawchuk, "Parametric Modeling of Lenslet-Array Optical Interconnections," Annual Meeting of the *Optical Society of America, paper* TuD3, Albuquerque, NM, Sept. 20-25, 1992.

56. A. Goldstein and B. K. Jenkins, "Optical Probability Density Function Estimation for Real-Time Pattern Classification," Annual Meeting of the *Optical Society of America, paper* ThQ3, Albuquerque, NM, Sept. 20-25, 1992.

57. P. Asthana, G. P. Nordin, A. R. Tanguay, Jr., and B. K. Jenkins, "Analysis of Weighted Fan-out/Fan-in Volume Holographic Interconnections," *Applied Optics,* **32** (8).PP. 1441-1469, March 1993)

58. D. Wiley, I. Glaser, B. K. Jenkins, and A. A. Sawchuk, "Incoherent Dynamic Lenslet Array Processors," accepted for publication in *Applied Optics.*

59. "Optical Nonlinear Neurons and Dynamic Interconnections using the Field Shielding Nonlinearity in CdTe," with M. Ziari, presented at 1989 Topical Meeting in Optical Computing, Salt Lake City, Utah (February 1989).

60. "Dynamic Optical Interconnection Branch Device Using the Optically-Controlled Nonuniform Electric Field Distribution inCdTe, with M. Ziari. Paper MBB6, Optical Society of America, Orlando, FL (October 1989).

61. "Infrared Nonlinear Neurons Using the Field Shielding Effect in CdTe," M. Ziari, and R. L. S. Devine, Applied Optics; special issue in Optical Computing 29,,2074-2083, (1990).

62. "Nonlinear Neurons Using the Field Shielding Effect in Photo-refractive CdTe," M. Ziari, and R. L. S. Devine. Photorefractive Materials, Effects and Devices II Conference, Aussois, France (January 1990).

63. "Photorefractivity at 1.5um in CdTe: V," with Afshir Partovi, James Millerd, Elsa Garmire, and Mehrdad Ziari. Photorefractive Materials, Effects and Devices II Conference, Aussois, France (January 1990).

64. "Photorefractivity at 1.5 um in CdTe:V", A. Partovi, J. Millerd, E. M. Garmire, M. Ziari, W. H. Steier, S. B. Trivedi, and M. B. Klein, Appl. Phys. Lett., 57, 846 (1990).

65. "Photorefractive Properties of CdTe:V at 1.5 um" M. Ziari, W. H. Steier, A. Partovi, J. Miller, E. Garmire, and M. Klein, Nonlinear Optics Conference, July 16-20, 1990, Kauai, Hawaii.

66. "Obervation of the Photorefractive ERffect in Vanadium Doped ZnTe", M. Ziari, W. H. Steier, P. M. Ranon, M. B. Klein, and S. Trevedi, OSA Meeting, San Jose, CA, Nov. 1991.

67. "Photorefractive Properties and Alternating Elective Field Gain Enhancement of Vanadium Doped Cadmium Telluride and Related Compounds," M. Ziari, W. H. Steier, M. B. Klein, and S. Trivedi,Topical Meeting on Photorefractivity, Beverly, Mass, July 29-31, 1991

68. "Photorefractivity in Vanadium-doped ZnTe", M. Ziari, W. H. Steier, P. M. Ranon, S. Trivedi, and M. B. Klein,Appl. Phys. Lett., 60, 1052-4, (1992).

69. "Enhancement of the Photorefractive Gain at 1.5 - 1.3 um in CdTe Using Alternating Electric Fields", M. Ziari, W. H. Steier, P. M. Ranon, M. B. Klein, and S.Trivedi, JOSA B, 9, August, 1992

70. "Photorefractive Effect in ZnTe" M. Ziari, W. H. Steier, P. Ranon, M. B. Klein, and S. Trevidi, presented at CLEO, Anaheim, Cal., May 1992.

71. "Optically Controlled Space Charge Fields Under the Electrode Region in Cadmium Telluride", M. Ziari and W. H. Steier, Paper D5.2, `Matr. Res. Soc. Mtg., San Francisco, May, 1992.

72. "Optical switching in cadmium telluride using a light-induced electrode nonlinearity", M. Ziari and W. H. Steier, Applied Optics., Oct. 1993

73. "Enhancement of the Photorefractive Gain in CdTe at 1.3-1.5 um under Alternating Elecrtic Fields", M. Ziari, W. H. Steier, P. M. Ranon, M. B. Klein, and S. Trevedi, OSA Meeting, Albuquerque, N. M., Sept. 1992.

74. P. Asthana, "Volume Holographic Techniques For Highly Multiplexed Interconnection Applications," Ph.D. Dissertation, University of Southern California, Los Angeles, California, (1991).

75. P. Asthana, E. J. Herbulock, Z. Karim, C. Kyriakakis, G. P. Nordin, and A. R. Tanguay, Jr., "Electrooptic Materials Requirements for Optical Information Processing and Computing," Materials Research Society Proceedings, Vol. 228 (1992), for the 1991 MRS Spring Meeting; (Invited Paper).

76. K. Hu, L. Chen, A. Madhukar, P. Chen, K. C. Rajkumar, K. Kaviani, Z. Karim, C. Kyriakakis, and A. R. Tanguay, Jr., "High Contrast Ratio Asymmetric Fabry-Perot Reflection Spatial Light Modulator Based on GaAs/InGaAs Multiple Quantum Wells," Appl. Phys. Lett., **59**(9), pp. 1108-1110 (1991).

77. K. Hu, L. Chen, A. Madhukar, P. Chen, C. Kyriakakis, Z. Karim, and A. R. Tanguay, Jr., "Inverted Cavity GaAs/InGaAs Asymmetric Fabry-Perot Reflection Modulator," Appl. Phys. Lett., **59**(14), pp 1664-1666 (1991).

78. K. Hu, L. Chen, R. Kapre, K. C. Rajkumar, A. Madhukar, Z. Karim, C. Kyriakakis, and A. R. Tanguay, Jr., "The Growth and Performance of Strained InGaAs/GaAs Multiple Quantum Well Based Asymmetric Fabry-Perot Reflection Modulators", Proc. of the IEEE-LEOS 1991 Summer Topical Meeting, (July 29-31, 1991, Newport Beach, CA), p. 18.

79. S. Piazzolla, B. K. Jenkins, and A. R. Tanguay, Jr., "A Single-Step Copying Process for Multiplexed Volume Holograms", Optics Letters, **17**, pp. 676-678, (1992).

80. G. P. Nordin, "Volume Diffraction Phenomena for Photonic Neural Network Implementations and Stratified Volume Holographic Optical Elements", Ph.D. Dissertation, University of Southern California, Los Angeles, California, (1992).

81. A. R. Tanguay, Jr., A. Madhukar, and B. Keith Jenkins. "Hybrid Silicon/Gallium Arsenide Inverted Fabry-Perot Cavity MQW Spatial Light Modulators", in *Spatial Light Modulators and Applications Technical Digest, 1993*, (Optical Society of America, Washington, D.C., 1993), p. 127.

82. Z. Karim, C. Kyriakakis, A. R. Tanguay, Jr., K. Hu, L. Chen, and A. Madhukar, "Externally-Deposited Phase-Compensating Dielectric Mirrors for Asymmetric Fabry-Perot Cavity Tuning", submitted to Applied Physics Letters, (1993).

83. Z. Karim, C. Kyriakakis, A. R. Tanguay, Jr., K. Hu, L. Chen, and A. Madhukar, "Ex-Situ Cavity Tuning of an Inverted Asymmetric Fabry-Perot InGaAs/GaAs Spatial Light Modulator Using an External Phase-Compensating Dielectric Mirror", submitted to Applied Physics Letters, (1993).

84. P. Asthana, G. P. Nordin, A. R. Tanguay, Jr., and B. K. Jenkins, "Beam Degeneracy Crosstalk in Fan-Out/Fan-In Volume Holographic Interconnections", in preparation for Optics Letters.

85. J. H. Rilum, and A. R. Tanguay, Jr., "Differential Interferometric Readout of Optical Disk Spatial Light Modulators", in preparation for Optics Letters.

86. J. H. Rilum and A. R. Tanguay, Jr., "Characterization of Optical Memory Disc Spatial Light Modulators for Optical Information Processing Applications", in preparation for Applied Optics.

87. C. Kyriakakis, Z. Karim, J. H. Rilum, J. J. Jung, A. R. Tanguay, Jr., and A. Madhukar, "Fundamental and Technological Limitations of Asymmetric Cavity MQW InGaAs/GaAs Spatial Light Modulators", in preparation for IEEE Journal of Quantum Electronics.

Patents

1. B. K. Jenkins and A. R. Tanguay, Jr., "Incoherent/Coherent Multiplexed Holographic Recording for Photonic Interconnections and Holographic Optical Elements", U.S. Patent No. 5,121,231, June 9, 1992.

2. B. K. Jenkins and A. R. Tanguay, Jr., "Incoherent/Coherent Source Array for Multiplexed Holographic Recording and Readout", filed 13 Feb 1992, U.S. Patent and Trademark Office, pending.

3. B. K. Jenkins and A. R. Tanguay, Jr., "Spatial Light Modulator for Incoherent/Coherent Multiplexed Holographic Recording and Readout", filed 13 Feb. 1992, U.S. Patent and Trademark Office, pending.